Taking the halogen bonding-hydrogen bonding competition one step further : complexes of difluoroiodomethane with trimethylphosphine, dimethyl sulfide and chloromethane

Taking the halogen bonding-hydrogen bonding competition one step further: Complexes of difluoroiodomethane with trimethylphosphine, dimethyl sulfide and chloromethane

Yannick Geboes[a,b], Frank De Proft[b] and Wouter A. Herrebout[a]*

[a] *Department of Chemistry, University of Antwerp, Groenenborgerlaan 171, 2020 Antwerp (Belgium), E-mail: Wouter.herrebout@uantwerpen.be*
[b] *Eenheid Algemene Chemie (ALGC), Member of the QCMM VUB-UGent Alliance Research Group, Vrije Universiteit Brussel (VUB), Pleinlaan 2, 1050 Brussels (Belgium)*

Corresponding Author:

W.A. Herrebout: e-mail: wouter.herrebout@uantwerpen.be, +32/3.265.33.73

Keywords: noncovalent interactions, halogen bonding, hydrogen bonding, FTIR, cryospectroscopy

Abstract

To rationalize the driving factors in the competition of halogen bonding and hydrogen bonding, the complexes of the combined halogen/hydrogen bond donor difluoroiodomethane with the Lewis bases trimethylphosphine, dimethyl sulfide and chloromethane are studied. For all Lewis bases, *ab initio* calculations lead to halogen and hydrogen bonded complexes. FTIR experiments involving solutions of mixtures of difluoroiodomethane with trimethylphosphine(-d_9) or dimethyl sulfide(-d_6) in liquid krypton confirm the coexistence of halogen bonded and hydrogen bonded complex. Also for solutions containing chloromethane, evidence for formation of binary associations is found, but no definitive assignment of the multiple complex bands could be made. Using van 't Hoff plots, the experimental complexation enthalpies for the halogen and hydrogen bonded complex of difluoroiodomethane with trimethylphosphine are determined to be -15.4(4) and -10.5(3) kJ mol^{-1}, respectively, while for the halogen and hydrogen bonded complexes with dimethyl sulfide, the values are and -11.3(5) and -7.7(6) kJ mol^{-1}, respectively. The experimental observation that for both trimethylphospine and dimethyl sulfide the halogen bonded complex is more stable than the hydrogen bonded complex supports the finding that softer Lewis bases tend to favor iodine halogen bonding over hydrogen bonding.

1. Introduction

In recent years, the competition between the halogen bonding and hydrogen bonding has been subject of various experimental and theoretical studies. (Perera *et al.*, 2016; Aakeroy *et al.*, 2015; Shirman *et al.*, 2015; Hogan & van Mourik, 2016; Domagała *et al.*, 2012; Oh *et al.*, 2012; Marti-Rujas *et al.*, 2012; Lieffrig *et al.*, 2012; Arman *et al.*, 2010; Minguez Espallargas *et al.*, 2009; Aakeröy *et al.*, 2009; Alkorta *et al.*, 2008; Aakeröy, Fasulo, *et al.*, 2007; Aakeröy, Desper, *et al.*, 2007; Zhu *et al.*, 2004; Corradi *et al.*, 2000) However, a systematic approach investigating the driving factors of the halogen bond-hydrogen bond competition at thermodynamic equilibrium is still absent. Recently, we have initiated an experimental study on the competition of these noncovalent interactions. In the first study by Nagels *et al.* (2014), experimental data on the different interactions present and their competition was obtained by studying the IR and Raman spectra of solutions in liquid krypton containing the combined hydrogen/halogen bond donor difluoroiodomethane (CHF_2I) and one of the Lewis bases trimethylamine (TMA), dimethyl ether (DME) or methyl fluoride (MF). For the solutions containing CHF_2I and TMA, it was found that the halogen bonded complex had a higher complexation enthalpy than the hydrogen bonded complex, whereas complexes of similar strength were found for the mixtures containing DME and only hydrogen bonded complex was observed in the solutions of MF. The experimental data were found to be in line with, *ab initio* calculations for complexes of CHF_2I with a series of lone pair containing Lewis bases suggesting that softer Lewis bases tend to favor C-I···Y halogen bonding over C-H···Y hydrogen bonding. To further build on this hypothesis, we have now expanded the experimental data towards complexes with additional (softer) Lewis bases containing a second period element with a lone pair, namely trimethylphosphine (TMP), dimethyl sulfide (DMS) and chloromethane (CH_3Cl). To avoid spectral congestion and aid assignment of the complex bands, measurements are performed using the regular (DMS, TMP) and fully deuterated (DMS-d_6, TMP-d_9) Lewis bases.

2. Experimental

The sample of difluoroiodomethane (CHF_2I, 97%) was purchased from ABCR and was used without further purification. Samples of dimethyl sulfide (DMS, 99%, anhydrous), trimethylphosphine (TMP, 99%), fully deuterated dimethyl sulfide (DMS-d_6, 99 atom% D) and fully deuterated trimethylphosphine (TMP-d_9, 99 atom% D) were purchased from Sigma-Aldrich and were transferred into a glass sample tube and degassed using a freeze-thaw cycle procedure. Chloromethane (CH_3Cl, 99.5%+) was purchased from Sigma-Aldrich and used without further purification. The solvent gas krypton was supplied by Air Liquide and had a stated purity of 99.9995%. When referring to (measurements or results of) both undeuterated and fully deuterated the notations TMP(-d_9) or DMS(-d_6) are used in the remainder of this paper.

The infrared spectra were recorded on a Bruker 66v FTIR spectrometer, equipped with a globar source, a Ge/KBr beam splitter and MCT detector, cooled with liquid nitrogen. Measurements were conducted in cells equipped with Si or ZnSe windows, with a path length of 10 mm and 20 mm respectively, to obtain spectra between 6500 cm^{-1} and 450 cm^{-1}. All interferograms were averaged over 500 scans, Blackman-Harris 3-term apodized and Fourier transformed with a zero filling factor of 8 to yield spectra with a resolution of 0.5 cm^{-1}.

Complexation stoichiometries were determined by performing an isothermal concentration study in which the concentrations of the solutes are systematically varied. By combining the Lambert-Beer law with the equilibrium constant for the formation of the complex A_mB_n

$$mA + nB \rightleftharpoons A_mB_n \quad (1)$$

it can be shown that the integrated intensity of a complex band is linearly related to the product of the *m*th power of the monomer intensity I_A and the *n*th power of monomer intensity I_B.

$$I_{A_mB_n} = C(I_A)^m(I_B)^n \quad (2)$$

where C is a constant related to the equilibrium constant. When plotting the integrated intensity of the complex $I_{A_mB_n}$ against the product of the integrated monomer intensities $(I_A)^x(I_B)^y$ a linear relationship will thus only be found when $x=m$ and $y=n$. (Herrebout, 2015) By preparing a series of plots for various integer values of *x* and *y* and evaluating their linearity, the complex stoichiometry can be established experimentally.

Estimated mole fractions of the solutions varied between 3.8×10^{-5} and 5.6×10^{-3} for CHF_2I, 9.4×10^{-4} and 4.7×10^{-3} for TMP, 1.9×10^{-3} and 5.6×10^{-3} for DMS and 2.3×10^{-4} and 2.1×10^{-2} for CH_3Cl and DME-d_6. As the experimental setup does not allow for verification of full solubility of the compounds, or verification of the fluid level in the filling tube, exact concentrations are not known.

Experimental complexation enthalpies were determined from van 't Hoff plots, based on measurements performed in the 120-156 K temperature interval. Using a subtraction procedure in which spectra of monomer solutions, recorded at identical temperatures and similar concentrations, are rescaled and subtracted from the spectrum of the mixture, a spectrum is obtained containing solely complex bands. (Herrebout, 2015) Band intensities are then integrated numerically, or are obtained from a band fit analysis in case both complex bands are not fully resolved, as is the case for the complex bands of ν_8 in mixtures with DMS(-d_6). Thermal expansion of the solvent gas during temperature studies was accounted for using the method published by van der Veken (1996).

To support our experimental measurements, *ab initio* MP2 calculations were performed using Dunning's augmented correlation consistent basis sets of double (aug-cc-pVDZ) or triple (aug-cc-pVTZ) zeta quality in Gaussian09. (Frisch *et al.*, 2009) The standard aug-cc-pVDZ and aug-cc-pVTZ basis sets were used for hydrogen, carbon, nitrogen, fluorine and chlorine, while aug-cc-pVDZ-PP and

aug-cc-pVTZ-PP basis sets including small-core energy-consistent relativistic pseudopotentials (PP) were used for bromine and iodine. (Feller, 1996; Schuchardt *et al.*, 2007) The counterpoise technique as proposed by Boys and Bernardi (1970) was used during all *ab initio* calculations to account for basis set superposition error. Energies at the basis set limit were calculated with Molpro (Werner *et al.*, 2012) using the extrapolation scheme of Truhlar (1998) in which the effect of electron correlation is obtained from MP2 calculations.

$$E_{CBS}^{HF} = \frac{3^{\alpha}}{3^{\alpha} - 2^{\alpha}} E_3^{HF} - \frac{2^{\alpha}}{3^{\alpha} - 2^{\alpha}} E_2^{HF} \quad (1)$$

$$E_{CBS}^{cor,MP2} = \frac{3^{\beta}}{3^{\beta} - 2^{\beta}} E_3^{cor,MP2} - \frac{2^{\beta}}{3^{\beta} - 2^{\beta}} E_2^{cor,MP2} \quad (2)$$

In these calculations α = 3.4 and β=2.2, (Truhlar, 1998) while energies with subscript 2 and 3 are calculated using the aug-cc-pVDZ(-PP) and aug-cc-pVTZ(-PP) basis sets respectively.

Furthermore, a correction for higher order correlation effects is made using the method of Jurečka and Hobza (2003), yielding results of $E_{CBS}^{CCSD(T)}$ quality.

$$\Delta E^{CCSD(T)} = \left| E^{CCSD(T)} - E^{MP2} \right|_{aug-cc-pVDZ(-PP)} \quad (3)$$

$$E_{CBS}^{CCSD(T)} = E_{CBS}^{HF} + E_{CBS}^{cor,MP2} + \Delta E^{CCSD(T)} \quad (4)$$

Complexation enthalpies in the vapor phase ΔH°(vap,calc) were obtained from the calculated complexation energies ΔE(CCSD(T)) by applying a zero-point energy correction and a correction for thermal effects, calculated at the MP2/aug-cc-pVDZ(-PP) level of theory. Correction of these calculated enthalpy values with solvent effects yields complexation enthalpies in solution ΔH°(LNg,calc) which can be compared with the experimental complexation enthalpies ΔH°(LNg). Corrections for thermal effects and zero-point vibrational contributions were obtained using statistical thermodynamics, whereas effects of solvation were accounted for using the Monte Carlo Free Energy Perturbation (MC-FEP) approach as implemented in an in-house modified version of BOSS 4.0. (Jorgensen, 1998)

3. Results

For both the complexes of CHF_2I with DMS and TMP, *ab initio* MP2/aug-cc-pVDZ-PP calculations lead to a stable halogen and hydrogen bonded complex geometry. For CH_3Cl, a single halogen bonded complex geometry and two different hydrogen bonded geometries are obtained. Apart from the C-H⋯Cl hydrogen bond, the latter geometries are discriminated by the appearance of an additional C-H⋯F or C-H⋯I secondary interaction, (*vide infra*). All complex geometries are shown in Figure 1, while Cartesian coordinates of all monomers and complexes are given in Tables S1 and S2 of the ESI. The intermolecular parameters and energetics for all complexes are summarized in Table 1.

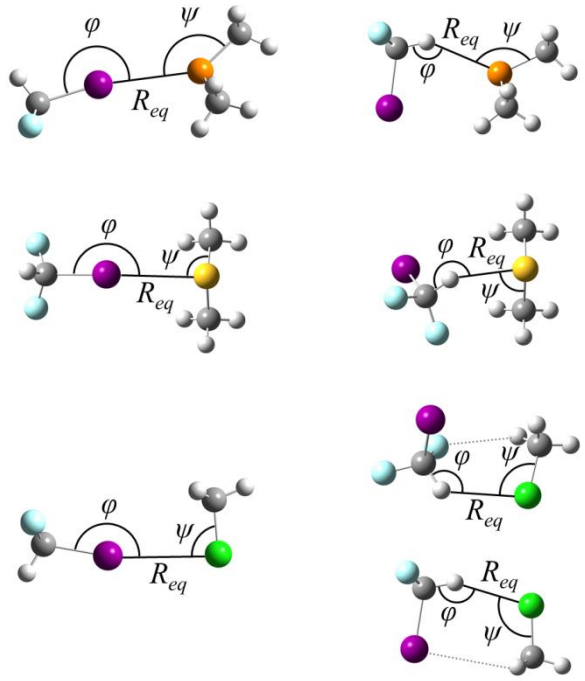

Figure 1: *Ab initio* calculated MP2/aug-cc-pVDZ-PP geometries for the XB (left) and HB (right) complexes of CHF_2I with TMP (top), DMS (middle) and CH_3Cl (bottom). For CH_3Cl, the hydrogen bonded complex with a secondary C-H···F interaction is shown on the top, while the hydrogen bonded complex with a secondary C-H···I interaction is shown in the bottom. Both secondary interactions are indicated by a grey dotted line.

Table 1: Intermolecular distance R_{eq} (Å), bond angles (°), MP2/aug-cc-pVDZ-PP ΔE(DZ) and CCSD(T)/CBS ΔE(CCSD(T)) extrapolated complexation energies, calculated vapor phase complexation enthalpies Δ*H*° (vap,calc), the calculated complexation enthalpies in liquid krypton (Δ*H*° (LKr,calc)) and the corresponding experimentally obtained complexation enthalpies (Δ*H*° (LKr)) (kJ mol^{-1}) for the complexes of CHF_2I with trimethylphosphine (TMP), dimethyl sulfide (DMS) and chloromethane (CH_3Cl). (X=H, I; Y=Cl, S, P)

	TMP		DMS		CH_3Cl		
	XB	HB	XB	HB	XB	HB (F)[b]	HB (I)[c]
$R_{eq}=R_{X\cdots Y}$ [a]	3.50	2.84	3.45	2.84	3.64	2.86	2.78
$\varphi_{C\text{-}X\cdots Y}$ [a]	170.38	145.23	170.29	128.49	169.11	125.86	153.09
$\psi_{C\text{-}Y\cdots X}$ [a]	143.66/103.84/103.83	131.27/111.66/111.66	90.77/90.77	97.02/110.20	86.39	99.55	107.93
Δ*E* (DZ)	-17.0	-18.9	-18.8	-18.9	-9.9	-12.9	-11.7
Δ*E* (CCSD(T))	-18.3	-20.4	-19.5	-20.6	-10.9	-14.6	-13.0
Δ*H*° (vap,calc)	-16.0	-17.8	-17.2	-18.0	-8.6	-12.1	-10.5
Δ*H*° (LKr,calc)	-14.9	-13.2	-15.3	-11.9	-7.1	-7.2	-6.9
Experimental							
Δ*H*° (LKr)	-15.4(4)	-10.5(3)	-11.3(5)	-7.7(6)			

[a] X = I, H, Y = Cl, S, P
[b] HB (F): hydrogen bonded complex with secondary C-H···F interaction,

[c] HB (I): hydrogen bonded complex with secondary C-H···I interaction.

For the halogen bonded complexes, geometries are found in which the C-I···Y angles are close to 170°. This is consistent with earlier observations that halogen bonds, due to the location and shape of the σ-hole in the electrostatic potential, form nearly linear complexes. (Metrangolo *et al.*, 2005) For the hydrogen bonded complexes, a larger deviation from linear behavior is observed, with C-H···Y bonding angles lying between 125.86° and 153.09°. This deviation can be explained by the possibility to form additional secondary stabilizing interactions with the Lewis base due to the absence of nonbonding valence electrons on the hydrogen atom, leading to a reduced directionality compared to halogen bonding. (Shields *et al.*, 2010) The presence of secondary interactions was studied using the noncovalent interactions index visualized using NCIPLOT (Johnson *et al.*, 2010; Contreras-García *et al.*, 2011). Plots of the reduced density gradient versus the electron density multiplied by the sign of the second Hessian eigenvalue and figures showing the gradient isosurfaces are given in Figures S1 to S3 of the ESI. For the complexes involving TMP, a single isosurface between iodine and phosphorus is observed for the halogen bonded complex, whereas in the hydrogen bonded complex, apart from the isosurface between the hydrogen and phosphorus atom, a second isosurface between iodine and the methyl groups of TMP is observed. In the hydrogen bonded complex with DMS an additional part of the isosurface is observed between the fluorine atom and the methyl group of DMS (at the backside of the image), explaining the tilted position of CHF_2I with a C-H···S angle of 128.49°. In the halogen bonded complex, two small circular isosurfaces are also observed between the fluorine atoms and the methyl groups of DMS. These surfaces are caused by the proximity of both entities due to the nearly perpendicular position of the lone pair on the sulfide atom to the C-S-C plane. For the halogen bonded complex with chloromethane a single isosurface is observed with an appendage between iodine and the methyl group due to the small C-Cl···I angle, a consequence of the accumulation of charge density perpendicular to the covalent bond. In the hydrogen bonded complexes additional isosurfaces between the methyl group and the fluorine or iodine atom are observed as the CHF_2I molecule is tilted towards CH_3Cl in both complexes. It is also noteworthy that the electrophilic donor molecule interacts with the chlorine atom almost perpendicular to the C-Cl bonding axis, the C-Cl···X bonding angles lying between 86.39° and 107.93°, due to the accumulated electron density in this region.

Comparison of the calculated complexation energies yields the a higher complexation energy for the hydrogen bonded complex than the halogen bonded complex for all three Lewis bases at all levels of theory. Upon application of the solvent effects from MC-FEP, this strength order changes for the complexes with TMP and DMS, whereas similar complex enthalpies are found for the complex with CH_3Cl.

To allow full characterization of the spectral features observed in the C-H stretching region of CHF_2I and avoid overlap with the modes from the Lewis bases, only spectra and assignments involving the deuterated Lewis bases DMS-d_6 and TMP-d_9 are reported in this study. Spectra and assignments of the non-deuterated species are included in Figures S4 and S5 and Tables S10 and S11 of the ESI. For CH_3Cl the non-deuterated species was used, as spectral congestion was not an issue for this Lewis base. The assignment of CHF_2I, (Nagels *et al.*, 2014) TMP, (McKean *et al.*, 1990) TMP-d_9, (Michielsen *et al.*, 2012) DMS (Hauchecorne *et al.*, 2011), DMS-d_6 (Michielsen *et al.*, 2012) and CH_3Cl (Futami *et al.*, 2004; Duncan & Law, 1990; Barnes *et al.*, 1973; Jones *et al.*, 1966) is primarily based on experimental studies available in the literature, aided by *ab initio* calculations, for which the results can be found in Tables S3 to S9 of the ESI.

In the spectra of mixtures with TMP-d_9 and TMP, shown in Figures 2 and S4 respectively, a clear distinction between both calculated complex geometries can be made in the C-F stretching region around 1100 cm^{-1}. In Panel 2B, spectra of the mixture (trace *a*), rescaled monomer spectra (traces *b* and *c*) and the resulting complex spectrum (trace *d*) is shown for this region. In trace *d*, the presence of both complex geometries is clearly visible for ν_8 ($\nu_{C\text{-}F,as}$) with redshifts of -19.9 cm^{-1} and -5.8 cm^{-1} for the XB and HB complex respectively. Also in the C-I stretching region and CF_2- bending region, shown in panels C and D respectively, two complex bands are observed with complexation shifts agreeing favorably with the calculated values. For the CHF_2I C-H stretching region shown in Panel A, however, no clear distinction between both complexes, which both have a predicted redshift, could be made. An overview of experimentally observed monomer bands, complexation shifts and the corresponding calculated shifts is given in Table 2 for TMP-d_9 and Table S10 for TMP.

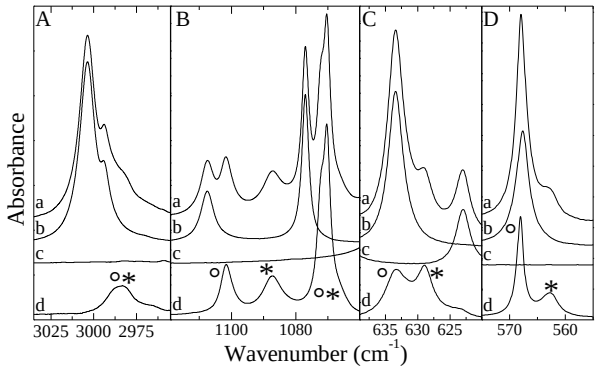

Figure 2: Infrared spectra of selected spectral regions for the mixtures of difluoroiodomethane with trimethylphosphine-d_9 dissolved in LKr at 130 K. In each panel, trace *a* represents the mixed solution, while traces *b* and *c* show the rescaled spectra of the solutions containing only difluoroiodomethane or trimethylphosphine-d_9, respectively. Trace *d* represents the spectrum of the complex which is obtained by subtracting the rescaled traces *b* and *c* from trace *a*. Bands due to the halogen and hydrogen bonded complexes observed in traces *d* are marked with an asterisk (*) or open circle (°), respectively. Estimated mole fractions of the solutions of the mixtures are 5.6×10^{-3} for CHF_2I and 2.8×10^{-3} for

TMP-d_9 in panel A, 5.6×10^{-5} for CHF_2I and 3.8×10^{-3} for TMP-d_9 in panel B, 6.6×10^{-5} for CHF_2I and 2.4×10^{-3} for TMP-d_9 in panel C and 1.9×10^{-3} for CHF_2I and 4.7×10^{-3} for TMP-d_9 in panel D.

As with the spectra from TMP-d_9, a clear distinction between both complex geometries formed with DMS-d_6 can be made when looking at the ν_8 mode of CHF_2I, shown in panel B of Figure 3, with a complexation shift of -14.7 cm^{-1} for the XB complex and -3.4 cm^{-1} for the HB complex. Also in the spectral region of the CF_2- bending mode, shown in Panel 3C, two complex bands are observed with shifts of 0.2 cm^{-1} and -3.0 cm^{-1}, corresponding to the HB and XB complex respectively. When looking to the CHF_2I C-H stretching mode (ν_1) for the mixture with DMS-d_6, shown in panel 3A, only a redshifted band is observed, even though a blueshift is predicted for the hydrogen bonded complex. An overview of experimentally observed monomer bands, complexation shifts and the corresponding calculated shifts is given in Table 3 for DMS-d_6 and Table S11 for DMS.

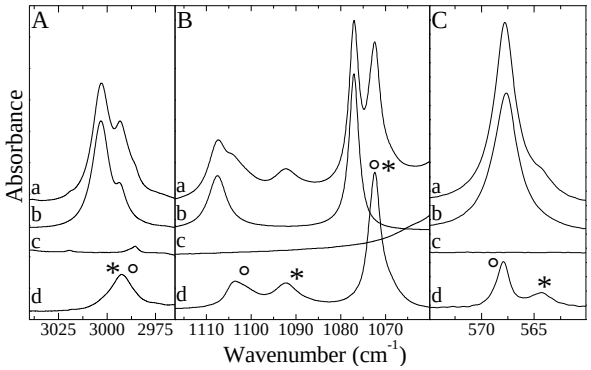

Figure 3: Infrared spectra of selected spectral regions for the mixtures of difluoroiodomethane with dimethyl sulfide-d_6 dissolved in LKr at 130 K. In each panel, trace *a* represents the mixed solution, while traces *b* and *c* show the rescaled spectra of the solutions containing only difluoroiodomethane or dimethyl sulfide-d_6, respectively. Trace *d* represents the spectrum of the complex which is obtained by subtracting the rescaled traces *b* and *c* from trace *a*. Bands due to the halogen and hydrogen bonded complexes observed in traces *d* are marked with an asterisk (*) or open circle (°), respectively. Estimated mole fractions of the solutions of the mixtures are 9.4×10^{-4} for CHF_2I and 1.9×10^{-3} for DMS-d_6 in panel A, 5.6×10^{-5} for CHF_2I and 5.6×10^{-3} for DMS-d_6 in panel B and 9.4×10^{-4} for CHF_2I and 1.9×10^{-3} for DMS-d_6 in panel C.

For the mixtures of CH_3Cl with CHF_2I, several complex bands are observed in multiple spectral region upon subtraction. For both the symmetrical and asymmetrical/antisymmetrical C-F stretches (ν_3 and ν_8), shown in Figure 4C, at least two redshifted bands are observed. The assignment of the complex bands to specific complex geometries is however complicated by the small values of the experimental and calculated complexation shifts for most bands, which is typical for rather weak noncovalent interactions. For the CHF_2I C-H stretching mode, shown in panel 4A, a redshift of -3.0 cm^{-1} is calculated for the XB complex whereas blueshifts of 15.7 cm^{-1} and 12.7 cm^{-1} are calculated for the HB

complexes. Upon inspection of the spectrum, a redshifted band is observed with a blueshifted shoulder on the left. Using a bandfit analysis, shifts of -0.4 cm^{-1} and 8.3 cm^{-1} were obtained. Due to the limited spectral intensity, which is consistent with the calculated low infrared intensities for the CHF_2I ν_1 mode in HB complexes given in Tables S7 and S8, the assignment of the HB complexes should be taken with the necessary prudence. For none of the complex bands of the CH_3Cl vibrational modes a distinction between the different geometries could be made experimentally. Furthermore, in none of the spectral regions complex bands were sufficiently resolved to construct a van 't Hoff plot to obtain complexation enthalpies of the complexes. An overview of experimentally observed monomer bands, complexation shifts and the corresponding calculated shifts for $CHF_2I{\cdot}CH_3Cl$ is given in Table 4.

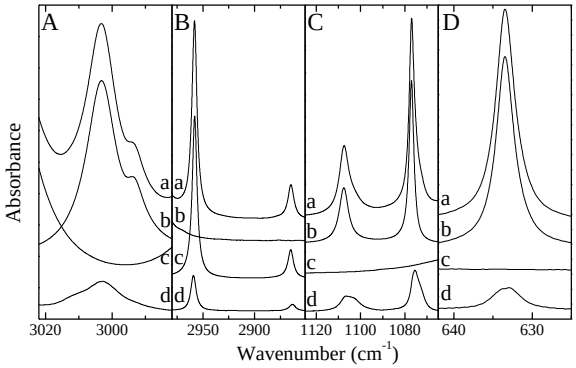

Figure 4: Infrared spectra of selected spectral regions for the mixtures of difluoroiodomethane with chloromethane dissolved in LKr at 130 K. In each panel, trace *a* represents the mixed solution, while traces *b* and *c* show the rescaled spectra of the solutions containing only difluoroiodomethane or chloromethane, respectively. Trace *d* represents the spectrum of the complex which is obtained by subtracting the rescaled traces *b* and *c* from trace *a*. Estimated mole fractions of the solutions of the mixtures are 9.4×10^{-3} for CHF_2I and 1.9×10^{-2} for CH_3Cl in panel A, 9.4×10^{-3} for CHF_2I and 2.3×10^{-3} for CH_3Cl in panel B, 5.6×10^{-5} for CHF_2I and 1.8×10^{-2} for CH_3Cl in panel C and 1.2×10^{-4} for CHF_2I and 1.9×10^{-2} for CH_3Cl in panel D.

Table 2: Experimental vibrational frequencies for the monomer and complexes, as well as experimental complexation shifts ($\Delta\nu_{exp}$) and MP2/aug-cc-pVDZ-PP calculated complexation shifts ($\Delta\nu_{calc}$), in cm^{-1}, for the halogen bonded complex (XB) and hydrogen bonded complex (HB) of difluoroiodomethane (CHF_2I) with trimethylphosphine-d_9 (TMP-d_9) dissolved in LKr at 130 K.

	Assignment	$\nu_{monomer}$	$\nu_{complex,XB}$	$\Delta\nu_{exp,XB}$	$\Delta\nu_{calc,XB}$	$\nu_{complex,HB}$	$\Delta\nu_{exp,HB}$	$\Delta\nu_{calc,HB}$
CHF_2I	ν_1	3003.3	2984.8	-18.5	-12.1	2984.8	-18.5	-19.6
	$\nu_5+\nu_7+\nu_8$	2993.9			-24.3			21.0
	$\nu_3+\nu_8$	2171.2	2144.0	-27.2	-23.4	2160.0	-11.2	-8.1
	$2\nu_3$	2144.1	2128.4	-15.7	-12.3	2134.2	-9.9	-7.8
	ν_7	1337.2	1335.6	-1.6	-2.3			23.5
	ν_2	1247.6	1243.5	-4.1	-1.1	1248.3	0.7	0.9
	ν_8	1107.6	1087.7	-19.9	-17.2	1101.8	-5.8	-4.2
	ν_3	1077.1	1070.5	-6.6	-6.1	1072.5	-4.6	-3.9

	ν_4	633.6	629.2	-4.4	-5.4	633.5	-0.1	-1.3
	ν_5	567.8	562.9	-4.9	-4.7	568.2	0.4	1.6
	$2\nu_6$	536.8			-7.6			-6.3
TMP-d_9	ν_{12}	2227.6	2229.8	2.2	2.3	2229.8	2.2	1.9
	ν_1	2217.1	2219.8	2.7	2.7	2219.8	2.7	2.4
	ν_{13}	2217.1	2219.8	2.7	2.8	2219.8	2.7	2.4
	ν_{14}	2219.5	2120.8	1.3	1.6	2120.8	1.3	1.5
	ν_2	2218.0	2119.5	1.5	1.6	2119.5	1.5	1.5
	ν_3	1047.8	1047.3	-0.5	-1.1	1074.3	-0.5	-0.4
	ν_{15}	1042.8	1042.1	-0.7	-1.1	1042.1	-0.7	-0.8
	ν_{16}	1035.4	1035.1	-0.3	-1.0	1035.1	-0.3	-0.4
	ν_4	1015.0	1016.3	1.3	0.3	1016.3	1.3	0.2
	ν_{17}	1004.3	1006.2	1.9	1.1	1006.2	1.9	0.7
	ν_5	782.5	782.6	0.1	0.2	782.6	0.1	1.5
	ν_{18}	756.6	759.3	2.7	3.0	759.3	2.7	2.3
	ν_{19}	646.1	651.3	5.2	5.7	649.9	3.8	3.9

Table 3: Experimental vibrational frequencies for the monomer and complexes, as well as experimental complexation shifts ($\Delta\nu_{exp}$) and MP2/aug-cc-pVDZ-PP calculated complexation shifts ($\Delta\nu_{calc}$), in cm^{-1}, for the halogen bonded complex (XB) and hydrogen bonded complex (HB) of difluoroiodomethane (CHF_2I) with dimethyl sulfide-d_6 (DMS-d_6) dissolved in LKr at 130 K.

	Assignment	$\nu_{monomer}$	$\nu_{complex,XB}$	$\Delta\nu_{exp,XB}$	$\Delta\nu_{calc,XB}$	$\nu_{complex,HB}$	$\Delta\nu_{exp,HB}$	$\Delta\nu_{calc,HB}$
CHF_2I	ν_1	3003.3	2992.8	-10.5	-9.3	2992.8	-10.5	9.7
	$\nu_{5+}\ \nu_{7+}\ \nu_8$	2993.9			-20.3			-3.8
	$\nu_{3+}\ \nu_8$	2170.7	2150.6	-20.1	-19.3	2162.3	-8.4	-8.0
	$2\nu_3$	2143.7	2131.0 [a]	-13.7	-9.4	2131.0 [a]	-13.7	-9.3
	ν_7	1337.3	1335.8	-1.5	-1.8	1335.8	-1.5	-1.1
	ν_2	1247.6	1247.8	0.2	-0.2	1247.8	0.2	-2.6
	ν_8	1107.3	1092.6	-14.7	-14.6	1103.9	-3.4	-3.4
	ν_3	1077.1	1072.4	-4.7	-4.7	1072.4	-4.7	-4.6
	ν_4	633.6	632.2	-1.4	-2.1	632.2	-1.4	-2.1
	ν_5	567.7	564.7	-3.0	-3.8	567.9	0.2	0.7
	$2\nu_6$	536.3	532.6	-3.7	-3.9	532.6	-3.7	-5.0
DMS-d_6	ν_1	2243.9	2246.3	2.4	1.9	2246.3	2.4	2.3
	ν_{16}	2243.9	2246.3	2.4	1.7	2246.3	2.4	1.2
	ν_{12}	2226.7	2230.2	3.5	2.8	2230.2	3.5	3.9
	ν_{17}	2131.6	2131.0	-0.6	-0.3	2131.0	-0.6	0.5
	ν_2	2129.7	2129.3	-0.4	-0.2	2131.0	1.3	0.8
	ν_3 (vw)	1064.3			-2.4			-1.1
	ν_{18}	1050.4	1048.4	-2.0	-2.3	1049.7	-0.7	-1.5
	ν_{13}	1044.4	1043.9	-0.5	-1.2	1043.9	-0.5	-2.1
	ν_4	1025.5	1025.4	-0.1	-1.4	1025.4	-0.1	-1.4
	ν_{19}	1009.0	1008.7	-0.3	-1.3	1008.7	-0.3	-1.4
	ν_5	828.1	828.0	-0.1	-0.3	828.0	-0.1	0.2
	ν_{14}	744.8	746.4	1.6	2.1	746.4	1.6	2.1
	ν_6	642.1	640.9	-1.2	-1.4	640.9	-1.2	-1.2

[a] overlap with complex band DMS-d_6 ν_{17}, ν_2

Table 4: Experimental vibrational frequencies for the monomer and complexes, as well as experimental complexation shifts ($\Delta\nu_{exp}$) and MP2/aug-cc-pVDZ-PP calculated complexation shifts ($\Delta\nu_{calc}$), in cm^{-1}, for the halogen bonded complex (XB) and hydrogen bonded complexes with a secondary C-H···F interaction (F) or secondary C-H···I interaction (I) of difluoroiodomethane (CHF_2I) with chloromethane (CH_3Cl) dissolved in LKr at 130 K.

	Assignment	$\nu_{monomer}$	$\nu_{complex,XB}$	$\Delta\nu_{exp,XB}$	$\Delta\nu_{calc,XB}$	$\nu_{complex,HB(F)}$	$\Delta\nu_{exp,HB(F)}$	$\Delta\nu_{calc,HB(F)}$	$\nu_{complex,HB(I)}$	$\Delta\nu_{exp,HB(I)}$	$\Delta\nu_{calc,HB(I)}$
CHF_2I	ν_1	3003.3	3002.9	-0.4	-3.0	3011.6	8.3	15.7	3011.6	8.3	12.7
	$\nu_5+\nu_7+\nu_8$	2993.9			-9.6			-6.1			10.4
	$\nu_3+\nu_8$	2171.2	2166.0	-5.2	-9.8	2166.0	-5.2	-9.4			-0.7
	$2\nu_3$	2144.1	2140.2	-3.9	-5.0	2133.9	-10.2	-12.6	2140.2	-3.9	-2.2
	ν_7	1337.2			-0.9			-3.2			8.7
	ν_2	1247.6	1249.4	1.8	1.5	1249.4	1.8	1.1	1247.3	-0.3	-0.6
	ν_8	1107.6	1103.0	-4.6	-7.3	1103.0	-4.6	-3.1	1107.0	-0.6	0.4
	ν_3	1077.1	1072.9	-1.5	-2.5	1072.9	-4.2	-6.3	1075.6	-1.5	-1.1
	ν_4	633.6	634.2	0.6	2.0	632.6	-1.0	-2.5	632.6	-1.0	-2.3
	ν_5	567.8	568.0	0.2	-1.4	568.0	0.2	0.2	568.0	0.2	1.4
	$2\nu_6$	536.8			2.0			-2.0			-4.1
CH_3Cl	ν_4[a]	3037.6									
	ν_4	3032.0	3033.9	1.9	2.2	3033.9	1.9	5.0	3033.9	1.9	5.5
	ν_1	2958.0	2959.2	1.2	-0.3	2959.2	1.2	1.7	2959.2	1.2	2.0
	$2\nu_5$	2865.3	2863.5	-1.8	-6.0	2863.5	-1.8	-4.9	2863.5	-1.8	-8.3
	ν_5	1444.5	1443.3[b]	-1.2	-3.0	1443.3[b]	-1.2	-2.5	1443.3[b]	-1.2	-4.2
	ν_2	1348.8	1349.1	0.3	-0.4	1349.1	0.3	0.3	1349.1	0.3	0.2
	ν_6	1016.2	1017.3	1.1	0.7	1017.3	1.1	2.2	1017.3	1.1	1.6
	ν_3 (^{35}Cl)	726.2	720.0	-6.2	-7.2	720.0	-6.2	-8.9	720.0	-6.2	-8.5
	ν_3 (^{37}Cl)	720.6	714.4	-6.2	-7.2	714.4	-6.2	-8.9	714.4	-6.2	-8.5

[a] Partially resolved dimer band (Futami *et al.*, 2004)

[b] Exact frequency could not be determined due to an impurity in the CHF_2I sample

To experimentally verify the complex stoichiometries of the complexes formed with TMP and DMS, concentration studies were performed at 130 K. The results are shown in Figures S6 to S9 of the ESI, and confirm a 1:1 complex stoichiometry for all four complexes.

Complexation enthalpies for the complexes with DMS and TMP were determined by measurements of solutions between 120 K and 156 K to create van 't Hoff plots. An illustration of these van 't Hoff plots is given in Figure S10 of the ESI. For the XB and HB complex of CHF_2I·TMP(-d_9), average complexation enthalpies of -15.4(6) kJ mol^{-1} and -10.5(3) kJ mol^{-1} respectively were determined in LKr. For the CHF_2I·DMS(-d_6) complexes average complexation enthalpies of -11.3(5) kJ mol^{-1} and -7.7(6) kJ mol^{-1} were determined in LKr. For mixtures of CHF_2I and CH_3Cl no complexation enthalpies could be determined due to a lack of separation of the observed complex bands. An overview of all experimental complexation enthalpies is given in Table 1.

4. Discussion

The spectral data reported above clearly illustrate the occurrence of halogen bonded and hydrogen bonded complexes in solutions of CHF_2I with TMP-(d_9). The experimental complexation enthalpies derived from the van 't Hoff plots, -15.4(4) kJ mol^{-1} for the XB complex and -10.5(3) kJ mol^{-1} for the HB complex, are in excellent agreement with the calculated values of -14.9 kJ mol^{-1} and -13.2 kJ mol^{-1}. This experimental data thus confirms the computational prediction that the XB complex is more stable than the HB complex in a LKr solution when using TMP as a Lewis base.

Also for the mixtures of CHF_2I with DMS or DMS-d_6, the presence of two different types of complexes can be deduced for several vibrational modes. By combining the experimental data with *ab initio* harmonic vibrational frequencies, the complex bands observed can be assigned confidently to the XB or the HB complex. The experimental complexation enthalpies derived from the van 't Hoff plots, -11.3(5) kJ mol^{-1} and -7.7(6) kJ mol^{-1}, again are in good agreement with the calculated values of -15.3 and -11.9 kJ mol^{-1}. As before, the XB complex is found to be the most stable complex geometry both experimentally and computationally.

One of the main discrepancies between the observed spectra and the calculated complexation shifts of the CHF_2I·DMS(-d_6) complexes is the absence of the blueshifted band in the CHF_2I C-H stretching region (ν_1) for the hydrogen bonded complex. Furthermore, the calculated blueshifted band for the hydrogen bonded complex also strongly contrasts with the data for TMP(-d_9), where both the calculations and the experiments lead to a weakening of the C-H bond and a redshift of its stretching frequency in the complex. The differences between experiment and theory can, in principle, be related to various phenomena including, amongst others, differences in anharmonicity perturbing the

frequencies in monomer and complexes. Also, different effects of solvation leading to the different solvent induced frequency shifts in the cryosolutions studied might be envisaged.

It should be noted that a very similar behavior as that observed for CHF_2I·DMS was also observed for the complexes of halothane ($CF_3CHBrCl$) with benzene by Michielsen *et al.* (2010), the blue- and redshift for the C-H stretching fundamental of halothane derived from the *ab initio* data and the spectroscopic data in liquid krypton being 10.2 and -1.1 cm^{-1}. Based on complementary data derived using FTIR and Raman studies of the same complex formed in supersonic jet expansion showing that at significantly lower temperatures a blueshift of 7.7 cm^{-1} is observed, the discrepancies between the cryosolution experiments and the calculated (*ab initio*) data was proposed to be due to the increase with temperature of the population of the low-frequency van der Waals modes of the complex. The driving force of the model is the observation that, due to strong anharmonicity of the van der Waals stretching mode, the molecules in the complex tend to move away from each other, yielding an intramolecular distance that on average is somewhat larger than that of the equilibrium geometry.

To support the idea that also in the hydrogen bonded complex of CHF_2I with DMS the complexation shift for the C-H stretching mode is largely affected by temperature effects, two different model calculations were initiated in this study. In the first approach, different geometries for the complex were obtained by changing the C···S intermolecular distance. Subsequently, for all geometries obtained, partial geometry optimizations were initiated in which the intermolecular distance was fixed and harmonic vibrational frequencies and complexation shifts were derived for all vibrational modes. Typical results for the CHF_2I ν_1 and ν_8 modes derived using this procedure are given in Figure 5. The data for the C-H stretching mode clearly illustrate that upon decreasing the C···S intermolecular distance, the blueshift for the C-H stretching mode is predicted to further increase, while an increase of the intermolecular distance first leads to a decrease of the blueshift and then changes it into a redshift. Most notably, the behavior of the CHF_2I ν_1 mode does not change continually, but rather jumps from -3.9 cm^{-1} to -13.0 cm^{-1} between 3.83 and 3.84 Å. Comparison of the geometries obtained shows that at this distance, the secondary C-H···F interaction is disrupted, causing the CHF_2I molecule to turn away from the DMS molecule, yielding a complex of C_s symmetry. The relationship between this change in geometry and frequency shift was further analyzed by freezing the C-H···S or C-H···S and C-H···S-C angles during optimization, which led to continuous C···S distance-ν_1 frequency curves with minima of -3.8 cm^{-1} and -3.0 cm^{-1} at a C···S distance of 4.3 Å, as shown in Figure S11 of the ESI. Furthermore, by restricting the HB complex to C_s symmetry during optimization, a redshift of -11.4 cm^{-1} is calculated with (3.63 Å) or without (3.77 Å) freezing of the C···S distance.

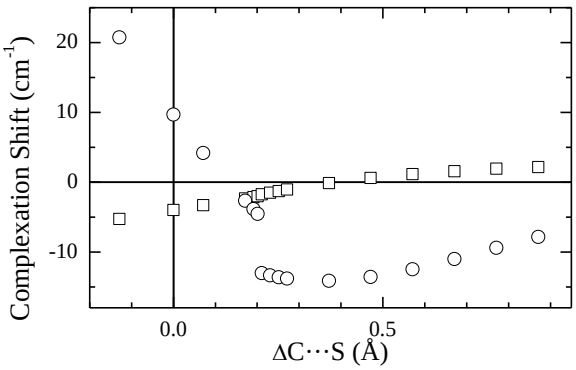

Figure 5: Complexation shifts (in cm^{-1}) of the CHF_2I ν_1 mode (○) and CHF_2I ν_8 mode (□) of the HB complex plotted against the change in C···S distance (in Å) as compared to the distance for the equilibrium geometry.

Comparison of the data for the CHF_2I ν_1 and ν_8 modes clearly shows that not all modes are affected in the same way. This observation is in line with the fact that in most cases a relatively good agreement is found between calculated and experimentally observed frequency shifts, and that only in specific cases, such as a CH stretching mode in blue-shifting hydrogen bonds, strong temperature effects could be expected to appear.

In the second model used, the above procedure was adopted to take into account the influence of the other van der Waals vibrations as well. To this end, a Monte Carlo simulation of the dynamical behavior of the complex was set up in which the intermolecular distance and the relative orientation of the rigid monomers were varied simultaneously, and the energy of the complex was calculated using MP2/aug-cc-pVDZ-PP calculations. Corrections for BSSE were avoided in order to keep the amount of CPU-time acceptable. Random distance variations between 0.05 to 0.15 Å and random angle variations between 5.0° to 15° resulted, *via* application of the Metropolis algorithm to the MP2 energies, in an acceptance ratio of 45%. Of the accepted structures, one in every 8 was used for further analysis. The latter consisted in optimizing the structure of both moieties of the complex, at the same level as above, while keeping the van der Waals parameters fixed. For the structure thus obtained, the C-H stretching frequency was determined by determining the corresponding Hessian. By using appropriate binning of the obtained frequencies, the distribution shown in Figure S12 of the ESI was obtained at a temperature of 130 K. The infrared intensity weighted average over the distribution yielded a complexation shift of the complex of -29.4 cm^{-1} for the C-H stretching mode, as compared to a shift of 9.7 cm^{-1} for the same mode in the equilibrium geometry. The data clearly shows that also in the second model, significant temperature effects are predicted and that also in this model, the blueshift obtained for the equilibrium geometry is converted in a redshift when temperature effects are corrected for. A further analysis of the data was not pursued, as all data were obtained without corrections for BSSE, and thus should only be considered as approximate.

When studying mixtures of CHF_2I with CH_3Cl, multiple complex bands are observed in several spectral regions, as shown in Figure 4. By comparing experimental complexation shifts with computational shifts, definitive assignment of all bands was deemed impossible, and the assignments given in Table 4 should thus be interpreted with the necessary prudence. Although it is clear that at least two different complexes are present in the solutions, the absence of the third complex geometry cannot be confirmed. Furthermore, due to the overlap of the complex bands in all observed spectral regions, no van 't Hoff plots could be constructed to aid the assignments.

Combining the experimental complexation enthalpies with those of the study involving methyl fluoride (CH_3F), dimethyl ether (DME) and trimethylamine (TMA), a halogen bond strength order N > P > O ≈ S is obtained for these Lewis bases, while the strength order for hydrogen bonding is found to be N > O ≈ P > S > F. It should be noted that these strength orders are in good agreement with the previously determined halogen bond strength order N > S > O and hydrogen strength order N > O > S. (Bent, 1968; Sheridan *et al.*, 1972; Martire *et al.*, 1976; Bertrán & Rodríguez, 1979, 1980)

From the previous results, it becomes abundantly clear that secondary interactions often play a major role in the competition of noncovalent interactions. The formation of secondary interactions in hydrogen bonded complexes is aided by two factors, when comparing to halogen bonded complexes. Firstly, the directionality of hydrogen bonds is far less stringent than in halogen bonds, which nearly always occur at a bonding angle approaching 180° as a consequence of the localization of the σ-hole, whereas hydrogen bond angles can be considerably less. (Legon, 2010, 2008; Politzer *et al.*, 2012; Shields *et al.*, 2010) Secondly, due to the increased size of the halogen atom as compared to hydrogen, the C-X···B bonding distance in halogen bonded complexes is significantly larger than the C-H···B bonding distance, which aids the formation of secondary interactions in the latter complexes. Even though the high directionality and lack of secondary interactions yields highly predictable structures for halogen bonded complexes, which is a major strong suit in several fields of applications such as crystal engineering, the lack of secondary interactions may well be their biggest weakness when having to compete with other noncovalent interactions, such as hydrogen bonds.

Apart from the ability to form secondary interactions, the chemical hardness/softness of the Lewis base also seems to play a major role in the competition of these noncovalent interactions, as mentioned in our previous study (Nagels *et al.*, 2014), which has shown that halogen bonding seems to prevail over hydrogen bonding when softer Lewis bases are involved. The results from this study support this finding, as the XB complex clearly prevails over the HB complex in mixtures of CHF_2I with TMP($-d_9$) or DMS($-d_6$), whereas a similar complexation enthalpy was found for the harder Lewis base DME. The ratio of the XB/HB complexation enthalpy rises from 1.29(3) for TMA($-d_9$) and 1.10(8) for DME($-d_6$) to 1.47(6) for TMP($-d_9$) and 1.47(13) for DMS($-d_6$) when descending from the second to third row of the periodic table. This seems consistent with the general HSAB theory, as the iodine

atom through which the halogen bond is formed is softer than the hydrogen atom. To evaluate this tendency, values for the chemical hardness of the different Lewis bases were calculated using the method of Tozer & De Proft (2005), based on the MP2/aug-cc-pVDZ(-PP) structures. An overview of the complexation enthalpies and chemical hardnesses for all Lewis bases is given in Table 5, while a plot of the the enthalpy ratio of $\frac{\Delta H°_{XB}}{\Delta H°_{HB}}$ versus chemical hardness η is given in Figure S13 of the ESI. From these data it becomes clear that for the three softest Lewis bases, with a nearly identical global chemical hardness, trimethylamine, trimethylphosphine and dimethyl sulfide, the complexation enthalpy of the halogen bonded complex is 1.29 to 1.47 times higher than for the hydrogen bonded complex, while for the slightly harder Lewis base dimethyl ether (η = 6.6 eV) this ratio diminishes to 1.10. For the hardest Lewis base studied, methyl fluoride (η = 8.5 eV), no halogen bonded complex was observed, (Nagels *et al.*, 2014) whereas for the slightly softer Lewis base methyl chloride (η = 7.1 eV) traces of halogen bonded complex are still observed. It should however be noted that this analysis is based on the use of the global hardness of the base. TMA and TMP, e.g., have almost the same global hardness, but one expects that locally, the nitrogen atom in TMA represents a harder site than the P atom in TMP, in accordance with the higher atomic hardness of N vs. P.

Table 5: Overview of the experimental complexation enthalpies (in kJ mol^{-1}) for the halogen ($\Delta H°_{XB}$) and hydrogen bonded complexes ($\Delta H°_{HB}$) with difluoroiodomethane in liquid krypton, enthalpy ratio $\frac{\Delta H°_{XB}}{\Delta H°_{HB}}$ and chemical hardness η (in eV) for trimethylamine (TMA), dimethyl ether (DME), methyl fluoride (CH_3F) , trimethylphosphine (TMP), dimethyl sulfide (DMS) and methyl chloride (CH_3Cl).

Lewis base	$\Delta H°_{XB}$ (LKr)	$\Delta H°_{HB}$ (LKr)	$\frac{\Delta H°_{XB}}{\Delta H°_{HB}}$	η (eV) [b]
TMA [a]	-19.0(3)	-14.7(2)	1.29(3)	5.6
DME [a]	-11.5(6)	-10.5(5)	1.10(8)	6.6
CH_3F [a]		-5.1(6)		8.5
TMP	-15.4(4)	-10.5(3)	1.47(6)	5.5
DMS	-11.3(5)	-7.7(6)	1.47(13)	5.7
CH_3Cl				7.1

[a] Results from Nagels *et al.* (2014).
[b] Calculated using the method described by Tozer and De Proft (2005)

In order to gain more insight into the driving forces of halogen and hydrogen bonding, an energy decomposition analysis was performed, for which details can be found in previous publications by Pinter *et al.* (2013); Nagels *et al.* (2014) and an overview of the results can be found in Table 6. From these data it is clear that the electrostatic (ΔV_{elst}) and orbital interaction (ΔE_{oi}) components of the interaction energy for the hydrogen bonded complexes increase towards the softer Lewis bases at the

bottom of the table. For the halogen bonded complexes this tendency is even more outspoken, the complex with TMA being an outlier. The stronger increase in ΔV_{elst} and ΔE_{oi} for the halogen bonded complex also means that these values are about 1.5-2 times higher than for the hydrogen bonded complexes for the softest Lewis bases DMS, TMA and TMP, whereas comparable values for ΔV_{elst} and ΔE_{oi} are found for the halogen and hydrogen bonded complexes with the hardest Lewis bases. When comparing ΔV_{elst} and ΔE_{oi} directly, it can be seen that the relative contribution of ΔE_{oi} increases towards the softer Lewis bases for both types of complexes, but remains consistently higher for the halogen bonded complexes as compared to the equivalent hydrogen bonded complexes. However, the Pauli repulsion energy (ΔE_{Pauli}) also increases more rapidly for the halogen bonded complex than the hydrogen bonded complex, thus reducing the effect of the increase in stabilization energy to the interaction energy (ΔE_{int}). Dispersion contributions remain relatively constant throughout the series of Lewis bases studied, although the contributions are consistently higher for the hydrogen bonded complexes, a consequence of the fact that they are more readily able to form secondary interactions than their halogen bonded counterparts, as shown in the NCI-plots in Figures S1-S3 of the ESI. Furthermore, as expected for relatively weak noncovalent interactions, all strain energies are negligible, the values being less than 1 kJ mol^{-1}. The negative strain energies for the hydrogen bonded complexes with CH_3Cl and TMP are a consequence of the difference in computational method used for the optimization (MP2/aug-cc-pVDZ-PP) and single point calculations in this analysis (PBE/TZ2P).

Table 6: Interaction energy (ΔE_{int}) and its components, ΔE_{Pauli}, ΔV_{elst}, ΔE_{oi} and dispersion (E_{disp}), strain energy ΔE_{strain} and complexation energy (ΔE^{DFT}) obtained at PBE/TZ2P level in kJ mol^{-1}.

	η (eV) [a]		ΔE_{Pauli}	ΔV_{elst} [b]	ΔE_{oi} [b]	E_{disp} [b]	ΔE_{int}	ΔE_{strain}	ΔE^{DFT}
CH_3F	8.5	HB (H···I)	9.1	-14.1 (70)	-6.0 (30)	-4.7	-15.6	0.4	-15.2
		HB (H···F)	9.1	-13.9 (73)	-5.2 (27)	-5.8	-15.8	0.6	-15.3
		XB	9.1	-11.3 (70)	-4.9 (30)	-3.1	-10.2	0.7	-9.6
CH_3Cl	7.1	HB (H···I)	9.0	-11.2 (63)	-6.5 (37)	-5.8	-14.6	-0.2	-14.7
		HB (H···F)	9.9	-12.1 (67)	-6.0 (33)	-7.2	-15.5	0.0	-15.5
		XB	11.4	-11.3 (61)	-7.2 (39)	-4.0	-11.0	0.1	-10.9
DME	6.6	HB	19.0	-23.0 (68)	-10.8 (32)	-8.7	-23.5	0.3	-23.2
		XB	29.1	-27.5 (65)	-15.0 (35)	-5.8	-19.1	0.8	-18.4
DMS	5.7	HB	17.8	-19.6 (63)	-11.4 (37)	-9.8	-23.0	0.0	-22.9
		XB	35.0	-29.6 (56)	-23.4 (44)	-6.1	-24.1	0.3	-23.9
TMA	5.6	HB	30.8	-33.5 (64)	-18.6 (36)	-9.5	-30.8	0.3	-30.7
		XB	75.4	-63.4 (63)	-37.1 (37)	-8.5	-33.7	0.6	-33.1
TMP	5.5	HB	19.8	-22.5 (62)	-13.8 (38)	-7.9	-24.3	-0.1	-24.4
		XB	37.3	-32.0 (56)	-24.8 (44)	-5.3	-24.7	0.4	-24.4

[a] Calculated using the method of Tozer and De Proft (2005)
[b] The relative contributions of the electrostatic and orbital interaction energies to the stabilization are indicated in brackets in percentages.

5. Conclusions

Ab initio calculations of the interactions between CHF_2I and TMP, DMS or CH_3Cl yielded both halogen bonded complexes and hydrogen bonded complexes for all three Lewis bases. For all Lewis bases, the highest complexation energies are found for the hydrogen bonded complexes at the MP2/aug-cc-pVDZ(-PP) and extrapolated CCSD(T)/CBS levels of theory. By application of solvent corrections and statistical thermodynamics, this strength order is reversed, yielding higher complex enthalpies in LKr for the halogen bonded complexes with TMP and DMS, as well as similar complex enthalpies for CH_3Cl. By analysis of the noncovalent index, the existence of secondary interactions in all three hydrogen bonded complexes is revealed, whereas these are absent in the halogen bonded complex geometries.

The experimental FTIR study of mixtures of CHF_2I with these Lewis bases in LKr, combined with the *ab initio* calculated frequency shifts revealed the coexistence of halogen and hydrogen bonded complex in mixtures of TMP($-d_9$) and DMS($-d_6$). For the mixtures involving CH_3Cl, no definitive assignment of the complex bands belonging to at least two complex isomers could be made. The absence of a blueshifted band for the CHF_2I C-H stretching mode in the mixtures of CHF_2I with DMS-d_6, corresponding to the hydrogen bonded complex, has been rationalized as a temperature dependent behavior due to the anharmonicity of the van der Waals stretching mode. Complexation enthalpies of -15.4(4) kJ mol^{-1} and -10.5(3) kJ mol^{-1} were determined for the halogen and hydrogen bonded complex of CHF_2I with TMP($-d_9$) respectively by construction of a van 't Hoff plot. For the halogen and hydrogen bonded complexes of CHF_2I with DMS($-d_6$), complexation enthalpies of -11.3(5) and -7.7(6) kJ mol^{-1} have been measured. These measurements confirm that the halogen bonded complexes have a higher complexation enthalpy than the corresponding hydrogen bonds, as predicted by the calculated complexation enthalpies.

The experimental complexation enthalpies further confirm the observation that softer Lewis bases tend to favor iodine halogen bonding over hydrogen bonding at thermodynamic equilibrium. Furthermore, it can be concluded that the lack of ability to form secondary interactions, due to its linearity and increased intermolecular distance, hinders halogen bonding in its competition with hydrogen bonded at equilibrium conditions.

Supporting Information Available:

MP2/aug-cc-pVDZ(-PP) cartesian coordinates, vibrational frequencies, IR and Raman intensities of all monomers and complexes, experimental frequencies of CHF_2I, TMP, DMS and observed complexes in LKr, overview of parameters used in van 't Hoff plots, NCI plots for all calculated complex geometries, IR spectra of the regions of interest for mixtures involving TMP or DMS, typical van 't

Hoff plots for the CHF_2I·TMP and CHF_2I·DMS XB and HB complexes, concentration study plots for the halogen and hydrogen bonded complexes with DMS and TMP, distribution of C-H stretching frequencies from the CHF2I·DMS-d_6 hydrogen bonded complex and plot of the enthalpy ratio versus the chemical hardness of the studied complexes.

Acknowledgements

Y.G. wishes to thank the FWO-Vlaanderen for a doctoral fellowship (11O9514N and 11O9516N). W.H. acknowledges financial support through FWO-Vlaanderen and the Special Research Fund BOF (UA). F.D.P. wishes to acknowledge FWO-Vlaanderen and the Free University of Brussels (VUB) for continuous support to the ALGC research group, in particular the VUB for a Strategic Research Program awarded to ALGC, started up at January 1, 2013. The Hercules foundation and the VSC are thanked for generously providing the required CPU resources. Nathan Schulpen is acknowledged for contributions in the early phase of this study.

Graphical abstract for Table of contents:

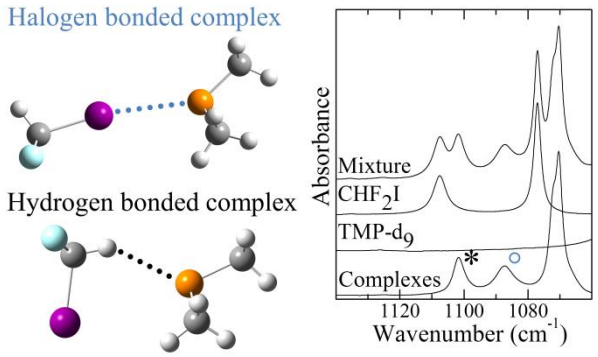

References:

Aakeröy, C. B., Desper, J., Helfrich, B. A., Metrangolo, P., Pilati, T., Resnati, G. & Stevenazzi, A. (2007). *Chem. Commun. (Cambridge, U. K.)* **41**, 4236-4238.

Aakeröy, C. B., Fasulo, M., Schultheiss, N., Desper, J. & Moore, C. (2007). *J. Am. Chem. Soc.* **129**, 13772-13773.

Aakeröy, C. B., Schultheiss, N., Rajbanshi, A., Desper, J. & Moore, C. (2009). *Cryst. Growth Des.* **9**, 432-441.

Aakeroy, C. B., Spartz, C. L., Dembowski, S., Dwyre, S. & Desper, J. (2015). *IUCrJ* **2**, 498-510.

Alkorta, I., Blanco, F., Solimannejad, M. & Elguero, J. (2008). *J. Phys. Chem. A* **112**, 10856-10863.

Arman, H. D., Gieseking, R. L., Hanks, T. W. & Pennington, W. T. (2010). *Chem. Commun.* **46**, 1854-1856.

Barnes, A. J., Hallam, H. E., Howells, J. D. R. & Scrimshaw, G. F. (1973). *J. Chem. Soc., Faraday Trans. 2* **69**, 738-749.

Bent, H. A. (1968). *Chem. Rev.* **68**, 587-648.

Bertrán, J. F. & Rodríguez, M. (1979). *Org. Magn. Reson.* **12**, 92-94.

Bertrán, J. F. & Rodríguez, M. (1980). *Org. Magn. Reson.* **14**, 244-246.

Boys, S. F. & Bernardi, F. (1970). *Mol. Phys.* **19**, 553-566.

Contreras-García, J., Johnson, E. R., Keinan, S., Chaudret, R., Piquemal, J.-P., Beratan, D. N. & Yang, W. (2011). *J. Chem. Theory Comput.* **7**, 625-632.

Corradi, E., Meille, S. V., Messina, M. T., Metrangolo, P. & Resnati, G. (2000). *Angew. Chem., Int. Ed.* **39**, 1782-1786.

Domagała, M., Matczak, P. & Palusiak, M. (2012). *Comput. Theor. Chem.* **998**, 26-33.

Duncan, J. L. & Law, M. M. (1990). *J. Mol. Spectrosc.* **140**, 13-30.

Feller, D. (1996). *J. Comp. Chem.* **17**, 1571-1586.

Frisch, M. J., Trucks, G. W., Schlegel, H. B., Scuseria, G. E., Robb, M. A., Cheeseman, J. R., Scalmani, G., Barone, V., Mennucci, B., Petersson, G. A., Nakatsuji, H., Caricato, M., Li, X., Hratchian, H. P., Izmaylov, A. F., Bloino, J., Zheng, G., Sonnenberg, J. L., Hada, M., Ehara, M., Toyota, K., Fukuda, R., Hasegawa, J., Ishida, M., Nakajima, T., Honda, Y., Kitao, O., Nakai, H., Vreven, T., Montgomery, J. A., Jr., Peralta, J. E., Ogliaro, F., Bearpark, M., Heyd, J. J., Brothers, E., Kudin, K. N., Staroverov, V. N., Kobayashi, R., Normand, J., Raghavachari, K., Rendell, A., Burant, J. C., Iyengar, S. S., Tomasi, J., Cossi, M., Rega, N., Millam, N. J., Klene, M., Knox, J. E., Cross, J. B., Bakken, V., Adamo, C., Jaramillo, J., Gomperts, R., Stratmann, R. E., Yazyev, O., Austin, A. J., Cammi, R., Pomelli, C., Ochterski, J. W., Martin, R. L., Morokuma, K., Zakrzewski, V. G., Voth, G. A., Salvador, P., Dannenberg, J. J., Dapprich, S., Daniels, A. D., Farkas, Ö., Foresman, J. B., Ortiz, J. V., Cioslowski, J. & Fox, D. J. (2009). *Gaussian 09, Revision D.01.*

Futami, Y., Kudoh, S., Ito, F., Nakanaga, T. & Nakata, M. (2004). *J. Mol. Struct.* **690**, 9-16.

Hauchecorne, D., Moiana, A., van der Veken, B. J. & Herrebout, W. A. (2011). *Phys. Chem. Chem. Phys.* **13**, 10204-10213.

Herrebout, W. A. (2015). *Top. Curr. Chem.* **358**, 79-154.

Hogan, S. W. L. & van Mourik, T. (2016). *J. Comput. Chem.* **37**, 763-770.

Johnson, E. R., Keinan, S., Mori-Sánchez, P., Contreras-García, J., Cohen, A. J. & Yang, W. (2010). *J. Am. Chem. Soc.* **132**, 6498-6506.

Jones, E. W., Popplewell, R. J. L. & Thompson, H. W. (1966). *Spectrochim. Acta* **22**, 669-680.

Jorgensen, W. L. (1998). *BOSS - Biochemical and Organic Simulation System*. New York: John Wiley & Sons Ltd.

Jurečka, P. & Hobza, P. (2003). *J. Am. Chem. Soc.* **125**, 15608-15613.

Legon, A. C. (2008). *Struct. Bond.* **126**, 17-64.

Legon, A. C. (2010). *Phys. Chem. Chem. Phys.* **12**, 7736-7747.

Lieffrig, J., Jeannin, O., Guizouarn, T., Auban-Senzier, P. & Fourmigué, M. (2012). *Cryst. Growth Des.* **12**, 4248-4257.

Marti-Rujas, J., Colombo, L., Lu, J., Dey, A., Terraneo, G., Metrangolo, P., Pilati, T. & Resnati, G. (2012). *Chem. Commun.* **48**, 8207-8209.
Martire, D. E., Sheridan, J. P., King, J. W. & O'Donnell, S. E. (1976). *J. Am. Chem. Soc.* **98**, 3101-3106.
McKean, D. C., McQuillan, G. P., Murphy, W. F. & Zerbetto, F. (1990). *J. Phys. Chem.* **94**, 4820-4831.
Metrangolo, P., Neukirch, H., Pilati, T. & Resnati, G. (2005). *Acc. Chem. Res.* **38**, 386-395.
Michielsen, B., Dom, J. J. J., van der Veken, B. J., Hesse, S., Xue, Z., Suhm, M. A. & Herrebout, W. A. (2010). *Phys. Chem. Chem. Phys.* **12**, 14034-14044.
Michielsen, B., Verlackt, C., van der Veken, B. J. & Herrebout, W. A. (2012). *J. Mol. Struct.* **1023**, 90-95.
Minguez Espallargas, G., Zordan, F., Arroyo Marin, L., Adams, H., Shankland, K., van de Streek, J. & Brammer, L. (2009). *Chem. - Eur. J.* **15**, 7554-7568.
Nagels, N., Geboes, Y., Pinter, B., De Proft, F. & Herrebout, W. A. (2014). *Chem. - Eur. J.* **20**, 8433-8443.
Oh, S. Y., Nickels, C. W., Garcia, F., Jones, W. & Friščić, T. (2012). *CrystEngComm* **14**, 6110-6114.
Perera, M. D., Desper, J., Sinha, A. S. & Aakeroy, C. B. (2016). *CrystEngComm* **18**, 8631-8636.
Pinter, B., Nagels, N., Herrebout, W. A. & De Proft, F. (2013). *Chem. - Eur. J.* **19**, 519-530.
Politzer, P., Riley, K. E., Bulat, F. A. & Murray, J. S. (2012). *Comput. Theor. Chem.* **998**, 2-8.
Schuchardt, K. L., Didier, B. T., Elsethagen, T., Sun, L., Gurumoorthi, V., Chase, J., Li, J. & Windus, T. L. (2007). *J. Chem. Inf. Model.* **47**, 1045-1052.
Sheridan, J. P., Martire, D. E. & Tewari, Y. B. (1972). *J. Am. Chem. Soc.* **94**, 3294-3298.
Shields, Z. P., Murray, J. S. & Politzer, P. (2010). *Int. J. Quantum Chem.* **110**, 2823-2832.
Shirman, T., Boterashvili, M., Orbach, M., Freeman, D., Shimon, L. J. W., Lahav, M. & van der Boom, M. E. (2015). *Cryst. Growth Des.* **15**, 4756-4759.
Tozer, D. J. & De Proft, F. (2005). *J. Phys. Chem. A* **109**, 8923-8929.
Truhlar, D. G. (1998). *Chem. Phys. Lett.* **294**, 45-48.
van der Veken, B. J. (1996). *J. Phys. Chem.* **100**, 17436-17438.
Werner, H.-J., Knowles, P. J., Knizia, G., Manby, F. R., Schütz, M., Celani, P., Korona, T., Lindh, R., Mitrushenkov, A., Rauhut, G., Shamasundar, K. R., Adler, T. B., Amos, R. D., Bernhardsson, A., Berning, A., Cooper, D. L., Deegan, M. J. O., Dobbyn, A. J., Eckert, F., Goll, E., Hampel, C., Hesselmann, A., Hetzer, G., Hrenar, T., Jansen, G., Köppl, C., Liu, Y., Lloyd, A. W., Mata, R. A., May, A. J., McNicholas, S. J., Meyer, W., Mura, M. E., Nicklass, A., O'Neill, D., Palmieri, P., Peng, D., Pflüger, K., Pitzer, R., Reiher, M., Shiozaki, T., Stoll, H., Stone, A. J., Tarroni, R., Thorsteinsson, T. & Wang, M. (2012). *MOLPRO, version 2012.1, A Package of Ab Initio Programs.*
Zhu, S., Xing, C., Xu, W. & Li, Z. (2004). *Tetrahedron Lett.* **45**, 777-780.

Taking the halogen bonding-hydrogen bonding competition one step further: Complexes of CHF_2I with trimethylphosphine, dimethyl sulfide and chloromethane

Yannick Geboes[a,b], Frank De Proft[b] and Wouter A. Herrebout[a]*

[a] *Department of Chemistry, University of Antwerp, Groenenborgerlaan 171, 2020 Antwerp (Belgium), E-mail: Wouter.herrebout@uantwerpen.be*
[b] *Eenheid Algemene Chemie (ALGC), Member of the QCMM VUB-UGent Alliance Research Group, Vrije Universiteit Brussel (VUB), Pleinlaan 2, 1050 Brussels (Belgium)*

Electronic supplementary information

Table S1.1: Cartesian coordinates of the MP2/aug-cc-pVDZ-PP optimized geometry of difluoroiodomethane.

	X	Y	Z
CHF_2I			
C	0.461801	-1.276126	0.000000
H	1.552810	-1.382611	0.000000
F	-0.060896	-1.882815	1.101579
F	-0.060896	-1.882815	-1.101579
I	-0.060896	0.810001	0.000000

Table S1.2: Cartesian coordinates of the MP2/aug-cc-pVDZ optimized geometry of trimethylphosphine.

	X	Y	Z
TMP			
P	0.000000	0.000000	0.618978
C	0.000000	1.626598	-0.285498
H	-0.889964	2.208825	-0.001487
H	0.889964	2.208825	-0.001487
H	0.000000	1.481355	-1.378927
C	-1.408675	-0.813299	-0.285498
H	-1.467917	-1.875144	-0.001487
H	-2.357881	-0.333681	-0.001487
H	-1.282891	-0.740678	-1.378927
C	1.408675	-0.813299	-0.285498
H	2.357881	-0.333681	-0.001487
H	1.467917	-1.875144	-0.001487
H	1.282891	-0.740678	-1.378927

Table S1.3: Cartesian coordinates of the MP2/aug-cc-pVDZ optimized geometry of dimethyl sulfide.

	X	Y	Z
DMS			
S	0.000000	0.674247	0.000000
C	-1.370330	-0.522675	0.000000
H	-2.309643	0.047454	0.000000
H	-1.334542	-1.152689	-0.900834
H	-1.334542	-1.152688	0.900834
C	1.370330	-0.522675	0.000000
H	1.334542	-1.152689	-0.900834
H	2.309643	0.047454	0.000000
H	1.334542	-1.152689	0.900834

Table S1.4: Cartesian coordinates of the MP2/aug-cc-pVDZ optimized geometry of chloromethane.

CH_3Cl	X	Y	Z

CH_3Cl			
C	0.000000	0.000000	-1.134242
H	0.000000	1.040001	-1.477217
H	-0.900667	-0.520001	-1.477217
H	0.900667	-0.520001	-1.477217
Cl	0.000000	0.000000	0.661006

Table S2.1: Cartesian coordinates of the MP2/aug-cc-pVDZ-PP optimized geometry of the hydrogen bonded complex between CHF_2I and trimethylphosphine.

	X	Y	Z
CHF_2I			
C	-1.216105	1.353406	-0.000007
H	-0.132928	1.531390	-0.000019
F	-1.797300	1.906772	-1.100901
F	-1.797275	1.906778	1.100897
I	-1.556091	-0.778530	0.000002
TMP			
P	2.433219	0.310927	-0.000005
C	2.626429	-0.879781	-1.413081
H	1.740677	-1.530608	-1.468765
H	2.700723	-0.323563	-2.360047
H	3.527461	-1.503794	-1.290861
C	4.140404	1.046128	-0.000009
H	4.271464	1.679600	-0.890422
H	4.271460	1.679624	0.890387
H	4.915127	0.261437	0.000003
C	2.626421	-0.879749	1.413099
H	2.700709	-0.323510	2.360052
H	1.740667	-1.530573	1.468791
H	3.527452	-1.503766	1.290898

Table S2.2: Cartesian coordinates of the MP2/aug-cc-pVDZ-PP optimized geometry of the halogen bonded complex between CHF_2I and trimethylphosphine.

	X	Y	Z
CHF_2I			
C	3.039329	0.000074	-0.120817
H	3.521408	0.000128	-1.106167
F	3.443285	-1.103496	0.579305
F	3.443117	1.103684	0.579340
I	0.894182	-0.000089	-0.330647
TMP			
P	-2.597960	-0.000069	-0.084146
C	-2.962250	1.415033	1.061597

H	-2.183466	1.468763	1.837625
H	-2.946416	2.360742	0.498785
H	-3.946593	1.299233	1.545139
C	-4.168149	-0.000761	-1.076796
H	-4.197578	0.889428	-1.723114
H	-4.197437	-0.891692	-1.722098
H	-5.055548	-0.000457	-0.422101
C	-2.962026	-1.413920	1.063213
H	-2.946027	-2.360269	0.501483
H	-2.183240	-1.466632	1.839308
H	-3.946393	-1.297731	1.546613

Table S2.3: Cartesian coordinates of the MP2/aug-cc-pVDZ-PP optimized geometry of the hydrogen bonded complex between CHF_2I and dimethyl sulfide.

	X	Y	Z
CHF_2I			
C	-0.785959	1.258032	-0.381791
H	0.079193	1.257115	-1.054250
F	-0.488219	1.947842	0.756259
F	-1.860138	1.858460	-0.964421
I	-1.281284	-0.778912	0.124298
DMS			
S	2.745384	0.432273	-0.507237
C	2.637149	0.518652	1.308262
H	2.514127	1.574865	1.584687
H	1.767347	-0.049505	1.669318
H	3.559797	0.130779	1.763817
C	2.888789	-1.375358	-0.664189
H	2.002971	-1.868460	-0.238243
H	2.953370	-1.612667	-1.735166
H	3.800441	-1.730811	-0.162384

Table S2.4: Cartesian coordinates of the MP2/aug-cc-pVDZ-PP optimized geometry of the halogen bonded complex between CHF_2I and dimethyl sulfide.

	X	Y	Z
CHF_2I			
C	-2.639583	0.000071	-0.002747
H	-3.199738	0.000218	-0.945700
F	-2.982435	-1.103272	0.727881
F	-2.982301	1.103281	0.728144
I	-0.520886	-0.000012	-0.388345
DMS			
S	2.929895	-0.000077	-0.424875
C	2.967183	1.372335	0.770366
H	2.930865	2.310712	0.199858
H	2.094133	1.323466	1.437999
H	3.896366	1.343011	1.357619
C	2.967139	-1.372225	0.770669
H	2.094094	-1.323176	1.438295
H	2.930784	-2.310727	0.200369
H	3.896326	-1.342805	1.357911

Table S2.5: Cartesian coordinates of the MP2/aug-cc-pVDZ-PP optimized geometry of the hydrogen bonded complex with a secondary C-H···F between CHF_2I and chloromethane.

	X	Y	Z
CHF_2I			
C	-0.341590	1.277646	-0.128791
H	0.442884	1.290430	-0.893239
F	-1.301935	2.198920	-0.414227
F	0.193498	1.594957	1.086312
I	-1.222580	-0.684963	-0.035059
CH_3Cl			
C	2.847452	-0.704367	0.946920
H	2.382405	0.045316	1.595374
H	3.855860	-0.952773	1.294024
H	2.222981	-1.601401	0.880877
Cl	2.990197	-0.003711	-0.704497

Table S2.6: Cartesian coordinates of the MP2/aug-cc-pVDZ-PP optimized geometry of the hydrogen bonded complex with a secondary C-H···I between CHF_2I and chloromethane.

	X	Y	Z
CHF_2I			
C	-0.676612	1.305798	-0.000004
H	0.402006	1.498825	-0.000030
F	-1.257116	1.857254	-1.101066
F	-1.257061	1.857249	1.101089
I	-1.011921	-0.824659	0.000000
CH_3Cl			
C	3.096877	-1.100970	0.000022
H	2.582231	-1.451300	-0.900496
H	2.582225	-1.451256	0.900554
H	4.146207	-1.414069	0.000033
Cl	3.060303	0.697955	-0.000023

Table S2.7: Cartesian coordinates of the MP2/aug-cc-pVDZ-PP optimized geometry of the halogen bonded complex between CHF_2I and chloromethane.

	X	Y	Z
CHF_2I			
C	2.439103	-0.010448	-0.000231
H	2.987805	-0.959635	-0.001505
F	2.782525	0.717958	-1.101619
F	2.782955	0.715250	1.102809
I	0.322673	-0.385166	-0.000280
CH_3Cl			
C	-3.173743	1.461749	0.000851

H	-4.185999	1.879482	0.001089
H	-2.627700	1.761309	-0.899947
H	-2.627660	1.760383	0.901930
Cl	-3.313505	-0.331435	-0.000066

Table S3A: MP2/aug-cc-pVDZ-PP vibrational frequencies, in cm^{-1}, infrared intensities, in km mol^{-1}, and Raman intensities, in $Å^4$ amu^{-1}, for the hydrogen bonded complex of CHF_2I and trimethylphosphine and both monomers, as well as the complexation shift $\Delta\nu$.

	Monomer			Hydrogen bonded complex			
	Frequency	IR intensity	Raman intensity	Frequency	$\Delta\nu$	IR intensity	Raman intensity
CHF_2I							
ν_1 (A')	3192.4	3.6	94.4	3172.8	-19.6	18.9	210.1
ν_2 (A')	1279.7	99.2	7.5	1280.3	0.6	129.6	31.5
ν_3 (A')	1074.1	300.4	3.2	1070.1	-3.9	309.6	3.5
ν_4 (A')	652.5	81.8	18.4	651.0	-1.5	72.8	10.9
ν_5 (A')	549.4	2.9	1.8	551.0	1.6	5.3	2.0
ν_6 (A')	276.0	0.2	6.6	272.7	-3.3	0.01	6.2
ν_7 (A")	1346.0	4.1	2.7	1369.5	23.5	8.9	1.0
ν_8 (A")	1096.9	186.9	1.9	1092.7	-4.2	164.9	1.5
ν_9 (A")	277.0	0.0004	1.2	275.5	-1.5	0.002	0.9
TMP							
ν_1 (A_1)	3148.5	33.6	160.8	3151.3	2.7	28.5	148.6
ν_2 (A_1)	3043.5	29.4	528.4	3045.9	2.3	30.0	526.0
ν_3 (A_1)	1469.0	9.2	1.5	1468.7	-0.3	8.0	0.9
ν_4 (A_1)	1314.7	5.1	7.3	1315.6	1.0	9.0	5.5
ν_5 (A_1)	957.8	20.1	5.0	959.4	1.5	34.9	4.2
ν_6 (A_1)	660.9	0.5	26.5	662.8	1.9	0.9	28.0
ν_7 (A_1)	287.5	1.0	1.5	287.8	0.3	0.9	1.4
ν_8 (A_2)	3168.1	0.0	0.0	3170.5	2.4	0.2	3.3
ν_9 (A_2)	1440.1	0.0	0.0	1439.3	-0.8	0.2	0.3
ν_{10} (A_2)	776.6	0.0	0.0	779.5	2.9	0.0001	0.03
ν_{11} (A_2)	164.1	0.0	0.0	164.5	0.4	0.007	0.01
ν_{12} (E)	3167.9	11.5	95.9	3170.2	2.3	8.6	78.4
ν_{13} (E)	3149.3	3.0	18.4	3152.4	3.1	2.6	23.2
ν_{14} (E)	3046.9	16.7	4.2	3049.3	2.4	14.1	14.8
ν_{15} (E)	1456.7	8.7	3.0	1456.0	-0.7	6.8	3.9
ν_{16} (E)	1446.2	3.1	9.5	1445.9	-0.3	2.6	8.4
ν_{17} (E)	1290.0	2.3	0.7	1290.6	0.7	2.4	0.7
ν_{18} (E)	946.6	16.5	0.5	948.9	2.3	16.4	0.9
ν_{19} (E)	831.0	0.2	0.3	833.2	2.2	0.2	0.4
ν_{20} (E)	718.3	11.6	11.8	722.8	4.5	9.4	13.0

ν_{21} (E)	249.8	0.2	2.8	248.2	-1.6	0.2	2.3
ν_{22} (E)	207.4	0.0009	0.6	207.3	-0.1	0.003	0.4

Van der Waals vibrations: 6.3 cm^{-1}, 0.07 km mol^{-1}, 0.1 $Å^4$ amu^{-1}, 27.1 cm^{-1}, 0.2 km mol^{-1}, 0.06 $Å^4$ amu^{-1}, 33.3 cm^{-1}, 0.2 km mol^{-1}, 0.5 $Å^4$ amu^{-1}, 46.7 cm^{-1}, 0.8 km mol^{-1}, 0.5 $Å^4$ amu^{-1}, 50.3 cm^{-1}, 0.8 km mol^{-1},
0.2 $Å^4$ amu^{-1}, 65.4 cm^{-1}, 0.2 km mol^{-1}, 0.7 $Å^4$ amu^{-1}.

Table S3B: MP2/aug-cc-pVDZ-PP vibrational frequencies, in cm^{-1}, infrared intensities, in km mol^{-1}, and Raman intensities, in $Å^4$ amu^{-1}, for the hydrogen bonded complex of CHF_2I and trimethylphosphine-d_9 and both monomers, as well as the complexation shift $\Delta\nu$.

	Monomer			Hydrogen bonded complex			
	Frequency	IR intensity	Raman intensity	Frequency	Δν	IR intensity	Raman intensity
CHF_2I							
ν_1 (A')	3192.4	3.6	94.4	3172.8	-19.6	17.5	200.9
ν_2 (A')	1279.7	99.2	7.5	1280.6	0.9	129.8	28.9
ν_3 (A')	1074.1	300.4	3.2	1070.2	-3.9	307.3	3.7
ν_4 (A')	652.5	81.8	18.4	651.2	-1.3	74.5	13.3
ν_5 (A')	549.4	2.9	1.8	551.0	1.6	5.3	2.0
ν_6 (A')	276.0	0.2	6.6	272.8	-3.2	0.008	6.5
ν_7 (A")	1346.0	4.1	2.7	1369.5	23.5	8.7	1.0
ν_8 (A")	1096.9	186.9	1.9	1092.7	-4.2	164.2	1.4
ν_9 (A")	277.0	0.0004	1.2	275.5	-1.5	0.002	0.9
TMP-d_9							
ν_1 (A_1)	2330.8	15.5	84.8	2333.2	2.4	13.1	87.2
ν_2 (A_1)	2184.5	10.3	254.0	2186.0	1.5	10.6	250.2
ν_3 (A_1)	1058.7	8.5	0.9	1058.4	-0.4	7.1	0.6
ν_4 (A_1)	1021.8	3.7	15.4	1022.0	0.2	6.6	16.3
ν_5 (A_1)	779.8	14.3	2.3	781.3	1.5	22.5	1.7
ν_6 (A_1)	597.0	0.0	20.0	598.6	1.6	0.2	18.6
ν_7 (A_1)	246.1	0.5	1.1	246.9	0.8	0.4	0.8
ν_8 (A_2)	2344.5	0.0	0.0	2346.4	1.9	0.001	0.2
ν_9 (A_2)	1041.0	0.0	0.0	1040.1	-0.9	0.002	0.2
ν_{10} (A_2)	582.2	0.0	0.0	584.4	2.3	0.002	0.02
ν_{11} (A_2)	116.8	0.0	0.0	117.2	0.4	0.003	0.006
ν_{12} (E)	2345.4	3.7	50.1	2347.3	1.9	2.9	43.6
ν_{13} (E)	2332.7	1.4	11.4	2335.1	2.4	1.0	12.2
ν_{14} (E)	2186.9	6.7	0.7	2188.5	1.5	5.5	5.3
ν_{15} (E)	1052.1	4.8	1.2	1051.3	-0.8	5.4	1.5
ν_{16} (E)	1044.7	0.2	4.5	1044.4	-0.4	0.2	3.9
ν_{17} (E)	1009.0	8.5	3.5	1009.7	0.7	8.9	3.5
ν_{18} (E)	760.6	15.4	1.8	762.9	2.3	15.1	2.7
ν_{19} (E)	652.0	3.6	6.9	655.9	3.9	1.9	7.7
ν_{20} (E)	625.1	0.5	0.7	626.6	1.5	0.2	0.8
ν_{21} (E)	208.8	0.1	2.3	207.9	-0.8	0.09	1.8
ν_{22} (E)	150.6	0.01	0.1	150.3	-0.2	0.01	0.1

Van der Waals vibrations: 5.9 cm^{-1}, 0.08 km mol^{-1}, 0.1 $Å^4$ amu^{-1}, 25.3 cm^{-1}, 0.1 km mol^{-1}, 0.04 $Å^4$ amu^{-1}, 32.2 cm^{-1}, 0.2 km mol^{-1}, 0.4 $Å^4$ amu^{-1}, 43.5 cm^{-1}, 0.7 km mol^{-1}, 0.5 $Å^4$ amu^{-1}, 45.3 cm^{-1}, 0.6 km mol^{-1}

[1],
0.2 $Å^4$ amu^{-1}, 63.6 cm^{-1}, 0.2 km mol^{-1}, 0.7 $Å^4$ amu^{-1}.

Table S4A: MP2/aug-cc-pVDZ-PP vibrational frequencies, in cm^{-1}, infrared intensities, in km mol^{-1}, and Raman intensities, in $Å^4$ amu^{-1}, for the halogen bonded complex of CHF_2I and trimethylphosphine and both monomers, as well as the complexation shift $\Delta\nu$.

	Monomer			Halogen bonded complex			
	Frequency	IR intensity	Raman intensity	Frequency	Δν	IR intensity	Raman intensity
CHF_2I							
ν_1 (A')	3192.4	3.6	94.4	3180.3	-12.1	8.7	168.9
ν_2 (A')	1279.7	99.2	7.5	1278.5	-1.2	147.4	9.0
ν_3 (A')	1074.1	300.4	3.2	1068.1	-6.0	349.6	4.6
ν_4 (A')	652.5	81.8	18.4	647.5	-5.0	45.4	95.4
ν_5 (A')	549.4	2.9	1.8	544.7	-4.7	2.7	6.1
ν_6 (A')	276.0	0.2	6.6	272.0	-4.0	4.5	31.1
ν_7 (A")	1346.0	4.1	2.7	1343.7	-2.3	4.2	3.6
ν_8 (A")	1096.9	186.9	1.9	1079.6	-17.2	183.7	1.7
ν_9 (A")	277.0	0.0004	1.2	278.6	1.6	0.04	1.5
TMP							
ν_1 (A_1)	3148.5	33.6	160.8	3151.6	3.1	31.3	188.2
ν_2 (A_1)	3043.5	29.4	528.4	3046.0	2.5	35.6	563.3
ν_3 (A_1)	1469.0	9.2	1.5	1467.7	-1.3	7.4	1.6
ν_4 (A_1)	1314.7	5.1	7.3	1315.4	0.7	3.9	17.1
ν_5 (A_1)	957.8	20.1	5.0	957.6	-0.3	72.2	22.1
ν_6 (A_1)	660.9	0.5	26.5	662.3	1.4	0.9	26.5
ν_7 (A_1)	287.5	1.0	1.5	286.2	-1.4	0.7	2.3
ν_8 (A_2)	3168.1	0.0	0.0	3170.0	1.9	3.9	32.9
ν_9 (A_2)	1440.1	0.0	0.0	1439.0	-1.1	0.01	0.05
ν_{10} (A_2)	776.6	0.0	0.0	779.1	2.6	0.0	0.01
ν_{11} (A_2)	164.1	0.0	0.0	163.9	-0.2	0.0008	0.002
ν_{12} (E)	3167.9	11.5	95.9	3170.9	3.0	6.2	65.4
ν_{13} (E)	3149.3	3.0	18.4	3152.8	3.5	2.3	29.9
ν_{14} (E)	3046.9	16.7	4.2	3049.4	2.5	13.4	18.5
ν_{15} (E)	1456.7	8.7	3.0	1455.5	-1.2	9.2	4.2
ν_{16} (E)	1446.2	3.1	9.5	1445.0	-1.2	2.2	8.5
ν_{17} (E)	1290.0	2.3	0.7	1290.9	0.9	4.0	1.2
ν_{18} (E)	946.6	16.5	0.5	948.9	2.3	16.0	0.8
ν_{19} (E)	831.0	0.2	0.3	832.1	1.2	0.8	0.6
ν_{20} (E)	718.3	11.6	11.8	724.7	6.4	8.7	16.0
ν_{21} (E)	249.8	0.2	2.8	245.3	-4.5	0.2	2.8
ν_{22} (E)	207.4	0.0009	0.6	207.0	-0.3	0.02	0.4

Van der Waals vibrations: 3.7 cm^{-1}, 1.0 km mol^{-1}, 0.009 $Å^4$ amu^{-1}, 12.0 cm^{-1}, 0.7 km mol^{-1}, 0.6 $Å^4$ amu^{-1}, 12.4 cm^{-1}, 1.5 km mol^{-1}, 0.5 $Å^4$ amu^{-1}, 52.0 cm^{-1}, 2.4 km mol^{-1}, 3.7 $Å^4$ amu^{-1}, 52.9 cm^{-1}, 0.004 km

mol^{-1},
0.2 $Å^4$ amu^{-1}, 57.7 cm^{-1}, 0.8 km mol^{-1}, 0.4 $Å^4$ amu^{-1}.

Table S4B: MP2/aug-cc-pVDZ-PP vibrational frequencies, in cm^{-1}, infrared intensities, in km mol^{-1}, and Raman intensities, in $Å^4$ amu^{-1}, for the halogen bonded complex of CHF_2I and trimethylphosphine-d_9 and both monomers, as well as the complexation shift $\Delta\nu$.

	Monomer			Halogen bonded complex			
	Frequency	IR intensity	Raman intensity	Frequency	Δν	IR intensity	Raman intensity
CHF_2I							
ν_1 (A')	3192.4	3.6	94.4	3180.3	-12.1	8.7	168.6
ν_2 (A')	1279.7	99.2	7.5	1278.6	-1.1	150.6	9.4
ν_3 (A')	1074.1	300.4	3.2	1067.9	-6.1	359.8	3.8
ν_4 (A')	652.5	81.8	18.4	647.2	-5.4	43.9	100.5
ν_5 (A')	549.4	2.9	1.8	544.7	-4.7	2.7	6.1
ν_6 (A')	276.0	0.2	6.6	272.2	-3.8	4.0	32.0
ν_7 (A")	1346.0	4.1	2.7	1343.7	-2.3	4.2	3.6
ν_8 (A")	1096.9	186.9	1.9	1079.6	-17.2	184.0	1.7
ν_9 (A")	277.0	0.0004	1.2	278.5	1.6	0.04	1.4
TMP-d_9							
ν_1 (A_1)	2330.8	15.5	84.8	2333.6	2.7	12.5	127.0
ν_2 (A_1)	2184.5	10.3	254.0	2186.1	1.6	12.7	263.2
ν_3 (A_1)	1058.7	8.5	0.9	1057.6	-1.1	9.3	0.7
ν_4 (A_1)	1021.8	3.7	15.4	1022.1	0.3	3.7	20.8
ν_5 (A_1)	779.8	14.3	2.3	780.1	0.2	46.1	10.8
ν_6 (A_1)	597.0	0.0	20.0	598.2	1.2	0.0	21.2
ν_7 (A_1)	246.1	0.5	1.1	245.7	-0.4	0.5	1.3
ν_8 (A_2)	2344.5	0.0	0.0	2346.3	1.8	0.5	6.4
ν_9 (A_2)	1041.0	0.0	0.0	1040.0	-1.0	0.0001	0.04
ν_{10} (A_2)	582.2	0.0	0.0	584.3	2.1	0.0003	0.008
ν_{11} (A_2)	116.8	0.0	0.0	116.7	-0.1	0.0004	0.001
ν_{12} (E)	2345.4	3.7	50.1	2347.7	2.3	2.2	39.4
ν_{13} (E)	2332.7	1.4	11.4	2335.4	2.8	0.7	14.5
ν_{14} (E)	2186.9	6.7	0.7	2188.5	1.6	5.1	6.1
ν_{15} (E)	1052.1	4.8	1.2	1051.0	-1.1	4.5	1.8
ν_{16} (E)	1044.7	0.2	4.5	1043.7	-1.0	0.2	4.0
ν_{17} (E)	1009.0	8.5	3.5	1010.1	1.1	8.0	5.0
ν_{18} (E)	760.6	15.4	1.8	763.7	3.0	13.5	3.3
ν_{19} (E)	652.0	3.6	6.9	657.7	5.7	3.6	5.7
ν_{20} (E)	625.1	0.5	0.7	625.6	0.5	0.3	1.6
ν_{21} (E)	208.8	0.1	2.3	206.0	-2.7	0.1	2.2
ν_{22} (E)	150.6	0.01	0.1	149.8	-0.8	0.04	0.1

Van der Waals vibrations: 3.6 cm^{-1}, 1.0 km mol^{-1}, 0.007 $Å^4$ amu^{-1}, 11.0 cm^{-1}, 0.6 km mol^{-1}, 0.6 $Å^4$ amu^{-1}, 11.4 cm^{-1}, 1.2 km mol^{-1}, 0.5 $Å^4$ amu^{-1}, 50.2 cm^{-1}, 2.5 km mol^{-1}, 3.5 $Å^4$ amu^{-1}, 50.8 cm^{-1}, 0.02 km mol^{-1}

[1],
0.1 $Å^4$ amu^{-1}, 54.9 cm^{-1}, 0.4 km mol^{-1}, 0.3 $Å^4$ amu^{-1}.

Table S5A: MP2/aug-cc-pVDZ-PP vibrational frequencies, in cm^{-1}, infrared intensities, in km mol^{-1}, and Raman intensities, in $Å^4$ amu^{-1}, for the hydrogen bonded complex of CHF_2I and dimethyl sulfide and both monomers, as well as the complexation shift $\Delta\nu$.

	Monomer			Hydrogen bonded complex			
	Frequency	IR intensity	Raman intensity	Frequency	Δν	IR intensity	Raman intensity
CHF_2I							
ν_1 (A')	3192.4	3.6	94.4	3202.1	9.7	3.0	99.6
ν_2 (A')	1279.7	99.2	7.5	1276.8	-2.9	100.4	17.0
ν_3 (A')	1074.1	300.4	3.2	1068.2	-5.9	269.8	3.3
ν_4 (A')	652.5	81.8	18.4	650.5	-2.0	72.7	14.0
ν_5 (A')	549.4	2.9	1.8	550.1	0.7	4.0	1.5
ν_6 (A')	276.0	0.2	6.6	273.5	-2.5	0.03	5.9
ν_7 (A")	1346.0	4.1	2.7	1344.4	-1.6	6.7	5.2
ν_8 (A")	1096.9	186.9	1.9	1092.9	-4.0	209.0	3.1
ν_9 (A")	277.0	0.0004	1.2	277.6	0.7	0.09	1.0
DMS							
ν_1 (A_1)	3186.3	9.8	92.1	3187.8	1.4	5.8	74.2
ν_2 (A_1)	3062.2	31.8	338.0	3063.7	1.5	24.5	329.7
ν_3 (A_1)	1473.5	0.3	7.6	1472.7	-0.8	2.1	7.8
ν_4 (A_1)	1352.5	0.8	0.9	1353.1	0.6	1.2	1.0
ν_5 (A_1)	1046.4	8.6	0.4	1047.9	1.5	8.0	0.3
ν_6 (A_1)	713.3	2.8	22.1	710.9	-2.4	2.8	19.3
ν_7 (A_1)	260.8	0.03	3.0	260.6	-0.2	0.05	2.4
ν_8 (A_2)	3168.0	0.0	16.5	3172.0	4.0	0.2	12.1
ν_9 (A_2)	1450.1	0.0	10.3	1448.3	-1.8	0.4	9.3
ν_{10} (A_2)	945.6	0.0	0.1	948.8	3.2	0.01	0.5
ν_{11} (A_2)	171.2	0.0	0.1	174.2	3.0	0.04	0.06
ν_{12} (B_1)	3159.9	21.3	119.4	3165.0	5.1	17.2	99.4
ν_{13} (B_1)	1462.5	12.9	0.02	1460.7	-1.8	10.7	0.5
ν_{14} (B_1)	982.7	4.1	0.006	985.7	3.0	10.9	0.4
ν_{15} (B_1)	187.1	0.8	0.09	188.5	1.4	1.1	0.1
ν_{16} (B_2)	3187.4	3.4	42.0	3190.0	2.6	2.7	43.4
ν_{17} (B_2)	3066.9	26.3	2.8	3068.0	1.1	20.5	6.1
ν_{18} (B_2)	1464.2	13.6	0.03	1462.9	-1.2	8.0	0.2
ν_{19} (B_2)	1326.0	6.5	0.1	1325.9	-0.1	4.2	0.1
ν_{20} (B_2)	912.7	0.2	0.2	915.2	2.5	0.1	0.1
ν_{21} (B_2)	765.1	0.1	8.5	762.7	-2.3	0.4	7.0

Van der Waals vibrations: 24.5 cm^{-1}, 0.6 km mol^{-1}, 0.5 $Å^4$ amu^{-1}, 31.4 cm^{-1}, 0.3 km mol^{-1}, 0.4 $Å^4$ amu^{-1}, 36.8 cm^{-1}, 1.1 km mol^{-1}, 0.2 $Å^4$ amu^{-1}, 61.8 cm^{-1}, 0.04 km mol^{-1}, 1.2 $Å^4$ amu^{-1}, 72.7 cm^{-1}, 0.3 km mol^{-1}

[1],
0.5 $Å^4$ amu^{-1}, 91.6 cm^{-1}, 7.3 km mol^{-1}, 0.2 $Å^4$ amu^{-1}.

Table S5B: MP2/aug-cc-pVDZ-PP vibrational frequencies, in cm^{-1}, infrared intensities, in km mol^{-1}, and Raman intensities, in $Å^4$ amu^{-1}, for the hydrogen bonded complex of CHF_2I and dimethyl sulfide-d_6 and both monomers, as well as the complexation shift $\Delta\nu$.

	Monomer			Hydrogen bonded complex			
	Frequency	IR intensity	Raman intensity	Frequency	Δν	IR intensity	Raman intensity
CHF_2I							
ν_1 (A')	3192.4	3.6	94.4	3202.1	9.7	2.9	99.6
ν_2 (A')	1279.7	99.2	7.5	1277.1	-2.6	101.4	16.0
ν_3 (A')	1074.1	300.4	3.2	1069.4	-4.6	254.4	3.3
ν_4 (A')	652.5	81.8	18.4	650.4	-2.1	73.4	13.1
ν_5 (A')	549.4	2.9	1.8	550.1	0.7	4.0	1.5
ν_6 (A')	276.0	0.2	6.6	273.5	-2.5	0.03	5.9
ν_7 (A")	1346.0	4.1	2.7	1344.9	-1.1	6.1	4.9
ν_8 (A")	1096.9	186.9	1.9	1093.5	-3.4	201.8	3.2
ν_9 (A")	277.0	0.0004	1.2	277.6	0.6	0.09	1.1
DMS-d_6							
ν_1 (A_1)	2361.4	4.6	45.5	2363.7	2.3	2.1	35.0
ν_2 (A_1)	2194.1	16.7	162.8	2195.0	0.8	12.9	158.2
ν_3 (A_1)	1064.3	0.5	3.0	1063.2	-1.1	13.1	3.4
ν_4 (A_1)	1037.4	1.2	5.6	1036.0	-1.4	0.3	5.5
ν_5 (A_1)	837.1	3.9	1.7	837.4	0.2	3.0	1.3
ν_6 (A_1)	655.7	2.7	17.4	654.5	-1.2	2.2	16.3
ν_7 (A_1)	223.6	0.0	2.2	223.7	0.1	0.05	1.8
ν_8 (A_2)	2350.5	0.0	8.5	2353.5	3.0	0.08	6.2
ν_9 (A_2)	1046.5	0.0	4.3	1044.4	-2.1	7.6	3.7
ν_{10} (A_2)	708.3	0.0	0.4	710.6	2.3	0.008	0.7
ν_{11} (A_2)	122.8	0.0	0.1	126.3	3.5	0.04	0.09
ν_{12} (B_1)	2344.4	10.8	63.9	2348.2	3.9	8.6	53.5
ν_{13} (B_1)	1056.3	7.2	0.0	1054.2	-2.1	17.7	0.4
ν_{14} (B_1)	751.1	0.9	0.1	753.2	2.1	2.8	0.4
ν_{15} (B_1)	136.8	0.8	0.1	139.4	2.6	1.9	0.1
ν_{16} (B_2)	2360.9	1.2	22.7	2362.1	1.2	1.6	25.8
ν_{17} (B_2)	2197.7	15.2	0.5	2198.2	0.5	11.8	2.4
ν_{18} (B_2)	1060.2	7.9	0.1	1058.7	-1.5	0.7	0.2
ν_{19} (B_2)	1017.4	2.5	0.6	1016.0	-1.4	0.9	0.5
ν_{20} (B_2)	720.2	0.0	7.3	718.8	-1.3	0.1	6.0
ν_{21} (B_2)	686.0	0.0	0.1	687.8	1.8	0.003	0.05

Van der Waals vibrations: 22.5 cm^{-1}, 0.5 km mol^{-1}, 0.4 $Å^4$ amu^{-1}, 31.0 cm^{-1}, 0.3 km mol^{-1}, 0.4 $Å^4$ amu^{-1}, 36.2 cm^{-1}, 1.0 km mol^{-1}, 0.2 $Å^4$ amu^{-1}, 54.5 cm^{-1}, 0.07 km mol^{-1}, 0.9 $Å^4$ amu^{-1}, 67.1 cm^{-1}, 0.9 km mol^{-}

[1],
0.5 Å^4 amu^{-1}, 83.8 cm^{-1}, 4.6 km mol^{-1}, 0.1 Å^4 amu^{-1}.

Table S6A: MP2/aug-cc-pVDZ-PP vibrational frequencies, in cm^{-1}, infrared intensities, in km mol^{-1}, and Raman intensities, in Å^4 amu^{-1}, for the halogen bonded complex of CHF_2I and dimethyl sulfide and both monomers, as well as the complexation shift $\Delta\nu$.

	Monomer			Halogen bonded complex			
	Frequency	IR intensity	Raman intensity	Frequency	Δν	IR intensity	Raman intensity
CHF_2I							
ν_1 (A')	3192.4	3.6	94.4	3183.2	-9.3	7.2	148.4
ν_2 (A')	1279.7	99.2	7.5	1279.5	-0.2	135.6	8.0
ν_3 (A')	1074.1	300.4	3.2	1069.0	-5.0	327.5	2.8
ν_4 (A')	652.5	81.8	18.4	650.5	-2.0	54.0	58.5
ν_5 (A')	549.4	2.9	1.8	545.6	-3.8	2.6	4.0
ν_6 (A')	276.0	0.2	6.6	274.1	-1.9	3.1	20.1
ν_7 (A")	1346.0	4.1	2.7	1344.2	-1.8	3.8	3.2
ν_8 (A")	1096.9	186.9	1.9	1082.2	-14.6	181.7	1.7
ν_9 (A")	277.0	0.0004	1.2	279.3	2.3	0.01	1.5
DMS							
ν_1 (A_1)	3186.3	9.8	92.1	3188.3	1.9	6.6	89.9
ν_2 (A_1)	3062.2	31.8	338.0	3062.3	0.1	24.3	311.5
ν_3 (A_1)	1473.5	0.3	7.6	1471.5	-2.0	2.8	9.7
ν_4 (A_1)	1352.5	0.8	0.9	1352.2	-0.3	0.2	7.5
ν_5 (A_1)	1046.4	8.6	0.4	1047.4	1.1	6.5	0.6
ν_6 (A_1)	713.3	2.8	22.1	710.5	-2.8	3.3	19.0
ν_7 (A_1)	260.8	0.03	3.0	261.1	0.3	0.03	2.5
ν_8 (A_2)	3168.0	0.0	16.5	3170.6	2.6	0.4	14.5
ν_9 (A_2)	1450.1	0.0	10.3	1448.3	-1.8	0.3	8.6
ν_{10} (A_2)	945.6	0.0	0.1	948.9	3.3	0.003	0.4
ν_{11} (A_2)	171.2	0.0	0.1	173.6	2.4	0.02	0.09
ν_{12} (B_1)	3159.9	21.3	119.4	3163.6	3.7	16.3	113.3
ν_{13} (B_1)	1462.5	12.9	0.02	1461.2	-1.4	13.6	0.5
ν_{14} (B_1)	982.7	4.1	0.006	984.9	2.3	13.6	0.7
ν_{15} (B_1)	187.1	0.8	0.09	188.0	0.9	1.8	0.4
ν_{16} (B_2)	3187.4	3.4	42.0	3189.3	1.9	1.7	32.6
ν_{17} (B_2)	3066.9	26.3	2.8	3066.7	-0.2	18.7	7.5
ν_{18} (B_2)	1464.2	13.6	0.03	1461.5	-2.6	8.0	0.4
ν_{19} (B_2)	1326.0	6.5	0.1	1326.0	0.1	3.5	0.09
ν_{20} (B_2)	912.7	0.2	0.2	914.9	2.2	0.2	0.2
ν_{21} (B_2)	765.1	0.1	8.5	762.3	-2.8	0.4	7.2

Van der Waals vibrations: 6.3 cm^{-1}, 2.5 km mol^{-1}, 0.05 $Å^4$ amu^{-1}, 32.2 cm^{-1}, 0.0002 km mol^{-1}, 1.0 $Å^4$ amu^{-1}, 32.5 cm^{-1}, 2.0 km mol^{-1}, 0.6 $Å^4$ amu^{-1}, 63.9 cm^{-1}, 1.5 km mol^{-1}, 1.8 $Å^4$ amu^{-1}, 67.2 cm^{-1}, 0.007 km mol^{-1}, 0.8 $Å^4$ amu^{-1}, 106.5 cm^{-1}, 12.3 km mol^{-1}, 2.9 $Å^4$ amu^{-1}.

Table S6B: MP2/aug-cc-pVDZ-PP vibrational frequencies, in cm^{-1}, infrared intensities, in km mol^{-1}, and Raman intensities, in $Å^4$ amu^{-1}, for the halogen bonded complex of CHF_2I and dimethyl sulfide-d_6 and both monomers, as well as the complexation shift $\Delta\nu$.

	Monomer			Halogen bonded complex			
	Frequency	IR intensity	Raman intensity				
CHF_2I							
ν_1 (A')	3192.4	3.6	94.4	3183.2	-9.3	7.2	148.8
ν_2 (A')	1279.7	99.2	7.5	1279.5	-0.2	136.1	7.9
ν_3 (A')	1074.1	300.4	3.2	1069.4	-4.7	311.5	2.1
ν_4 (A')	652.5	81.8	18.4	650.4	-2.1	52.9	60.6
ν_5 (A')	549.4	2.9	1.8	545.6	-3.8	2.6	4.0
ν_6 (A')	276.0	0.2	6.6	274.0	-1.9	3.1	20.0
ν_7 (A")	1346.0	4.1	2.7	1344.2	-1.8	3.9	3.2
ν_8 (A")	1096.9	186.9	1.9	1082.2	-14.6	181.4	1.7
ν_9 (A")	277.0	0.0004	1.2	279.3	2.3	0.01	1.5
DMS-d_6							
ν_1 (A_1)	2361.4	4.6	45.5	2363.2	1.9	2.9	46.5
ν_2 (A_1)	2194.1	16.7	162.8	2194.0	-0.2	13.0	148.8
ν_3 (A_1)	1064.3	0.5	3.0	1062.0	-2.4	20.4	5.5
ν_4 (A_1)	1037.4	1.2	5.6	1036.0	-1.4	0.6	9.2
ν_5 (A_1)	837.1	3.9	1.7	836.9	-0.3	2.6	1.5
ν_6 (A_1)	655.7	2.7	17.4	654.3	-1.4	4.6	13.0
ν_7 (A_1)	223.6	0.0	2.2	224.3	0.7	0.05	1.9
ν_8 (A_2)	2350.5	0.0	8.5	2352.4	1.9	0.2	7.2
ν_9 (A_2)	1046.5	0.0	4.3	1045.1	-1.4	0.2	3.6
ν_{10} (A_2)	708.3	0.0	0.4	710.9	2.6	0.004	0.8
ν_{11} (A_2)	122.8	0.0	0.1	126.4	3.6	0.01	0.1
ν_{12} (B_1)	2344.4	10.8	63.9	2347.2	2.8	7.8	58.6
ν_{13} (B_1)	1056.3	7.2	0.0	1055.1	-1.2	8.8	0.1
ν_{14} (B_1)	751.1	0.9	0.1	753.1	2.1	2.2	0.9
ν_{15} (B_1)	136.8	0.8	0.1	140.3	3.5	4.3	1.1
ν_{16} (B_2)	2360.9	1.2	22.7	2362.6	1.7	0.6	17.5
ν_{17} (B_2)	2197.7	15.2	0.5	2197.3	-0.3	10.9	3.0
ν_{18} (B_2)	1060.2	7.9	0.1	1057.9	-2.3	4.7	0.2
ν_{19} (B_2)	1017.4	2.5	0.6	1016.1	-1.3	1.7	0.5
ν_{20} (B_2)	720.2	0.0	7.3	718.5	-1.6	0.1	5.9
ν_{21} (B_2)	686.0	0.0	0.1	687.8	1.8	0.0008	0.1

Van der Waals vibrations: 6.0 cm^{-1}, 2.2 km mol^{-1}, 0.03 $Å^4$ amu^{-1}, 30.2 cm^{-1}, 0.002 km mol^{-1}, 1.0 $Å^4$ amu^{-1}, 31.4 cm^{-1}, 1.9 km mol^{-1}, 0.6 $Å^4$ amu^{-1}, 61.0 cm^{-1}, 0.009 km mol^{-1}, 0.5 $Å^4$ amu^{-1}, 61.3 cm^{-1}, 1.3

km mol^{-1},
1.6 Å^4 amu^{-1}, 94.9 cm^{-1}, 8.4 km mol^{-1}, 2.2 Å^4 amu^{-1}.

Table S7: MP2/aug-cc-pVDZ-PP vibrational frequencies, in cm^{-1}, infrared intensities, in km mol^{-1}, and Raman intensities, in $Å^4$ amu^{-1}, for the hydrogen bonded complex with a secondary C-H···F interaction of CHF_2I and chloromethane and both monomers, as well as the complexation shift $\Delta\nu$.

	Monomer			Hydrogen bonded complex (C-H···Cl + F···H-C)			
	Frequency	IR intensity	Raman intensity	Frequency	Δν	IR intensity	Raman intensity
CHF_2I							
ν_1 (A')	3192.4	3.6	94.4	3208.2	15.7	0.8	82.7
ν_2 (A')	1279.7	99.2	7.5	1280.8	1.1	101.4	8.9
ν_3 (A')	1074.1	300.4	3.2	1067.8	-6.3	266.0	3.0
ν_4 (A')	652.5	81.8	18.4	650.1	-2.5	75.2	15.9
ν_5 (A')	549.4	2.9	1.8	549.6	0.2	3.4	1.5
ν_6 (A')	276.0	0.2	6.6	275.0	-1.0	0.09	6.0
ν_7 (A")	1346.0	4.1	2.7	1342.8	-3.2	0.7	5.1
ν_8 (A")	1096.9	186.9	1.9	1093.8	-3.1	216.3	2.6
ν_9 (A")	277.0	0.0004	1.2	278.2	1.2	0.07	1.1
CH_3Cl							
ν_1 (A)	3109.9	24.4	147.2	3111.6	1.7	17.0	139.7
ν_2 (A)	1369.8	13.2	0.006	1370.0	0.3	11.1	0.1
ν_3 (A)	750.4	25.3	17.9	741.4	-8.9	23.8	14.7
ν_4 (E)	3230.5	3.6	48.9	3235.5	5.0	2.6	40.3
ν_5 (E)	1474.7	5.0	4.0	1472.3	-2.5	9.6	3.7
ν_6 (E)	1031.9	2.1	0.6	1034.2	2.2	3.5	0.6

Van der Waals vibrations: 22.8 cm^{-1}, 2.2 km mol^{-1}, 0.9 $Å^4$ amu^{-1}, 26.6 cm^{-1}, 0.8 km mol^{-1}, 0.5 $Å^4$ amu^{-1}, 41.9 cm^{-1}, 1.3 km mol^{-1}, 0.2 $Å^4$ amu^{-1}, 56.6 cm^{-1}, 0.3 km mol^{-1}, 0.2 $Å^4$ amu^{-1}, 70.2 cm^{-1}, 0.7 km mol^{-1},
0.3 $Å^4$ amu^{-1}, 80.7 cm^{-1}, 7.3 km mol^{-1}, 1.0 $Å^4$ amu^{-1}.

Table S8: MP2/aug-cc-pVDZ-PP vibrational frequencies, in cm^{-1}, infrared intensities, in km mol^{-1}, and Raman intensities, in $Å^4$ amu^{-1}, for the hydrogen bonded complex with a secondary C-H···I interaction of CHF_2I and chloromethane and both monomers, as well as the complexation shift $\Delta\nu$.

	Monomer			Hydrogen bonded complex (C-H···Cl + I···H-C)			
	Frequency	IR intensity	Raman intensity	Frequency	Δν	IR intensity	Raman intensity
CHF_2I							
ν_1 (A')	3192.4	3.6	94.4	3205.2	12.7	1.6	115.7
ν_2 (A')	1279.7	99.2	7.5	1279.1	-0.6	104.5	13.2
ν_3 (A')	1074.1	300.4	3.2	1073.0	-1.1	309.9	3.3
ν_4 (A')	652.5	81.8	18.4	650.2	-2.3	75.8	15.9
ν_5 (A')	549.4	2.9	1.8	550.8	1.4	4.5	1.8
ν_6 (A')	276.0	0.2	6.6	273.9	-2.1	0.04	6.3
ν_7 (A")	1346.0	4.1	2.7	1354.6	8.7	6.5	1.6
ν_8 (A")	1096.9	186.9	1.9	1097.2	0.4	176.1	1.8
ν_9 (A")	277.0	0.0004	1.2	276.2	-0.8	0.0	1.0
CH_3Cl							
ν_1 (A)	3109.9	24.4	147.2	3111.9	2.0	16.4	142.6
ν_2 (A)	1369.8	13.2	0.006	1369.9	0.2	12.0	0.1
ν_3 (A)	750.4	25.3	17.9	741.9	-8.5	24.1	14.5
ν_4 (E)	3230.5	3.6	48.9	3236.0	5.5	3.3	42.6
ν_5 (E)	1474.7	5.0	4.0	1470.6	-4.2	11.1	3.5
ν_6 (E)	1031.9	2.1	0.6	1033.6	1.6	3.1	0.6

Van der Waals vibrations: 5.7 cm^{-1}, 0.6 km mol^{-1}, 0.6 $Å^4$ amu^{-1}, 18.5 cm^{-1}, 3.7 km mol^{-1}, 0.1 $Å^4$ amu^{-1}, 28.5 cm^{-1}, 0.2 km mol^{-1}, 0.6 $Å^4$ amu^{-1}, 57.2 cm^{-1}, 0.04 km mol^{-1}, 0.03 $Å^4$ amu^{-1}, 61.1 cm^{-1}, 0.04 km mol^{-1},
0.4 $Å^4$ amu^{-1}, 72.2 cm^{-1}, 6.2 km mol^{-1}, 0.7 $Å^4$ amu^{-1}.

Table S9: MP2/aug-cc-pVDZ-PP vibrational frequencies, in cm^{-1}, infrared intensities, in km mol^{-1}, and Raman intensities, in $Å^4$ amu^{-1}, for the halogen bonded complex of CHF_2I and chloromethane and both monomers, as well as the complexation shift $\Delta\nu$.

	Monomer			Halogen bonded complex			
	Frequency	IR intensity	Raman intensity	Frequency	Δν	IR intensity	Raman intensity
CHF_2I							
ν_1 (A')	3192.4	3.6	94.4	3189.4	-3.0	4.6	113.8
ν_2 (A')	1279.7	99.2	7.5	1281.2	1.5	119.1	6.8
ν_3 (A')	1074.1	300.4	3.2	1071.6	-2.5	312.1	2.8
ν_4 (A')	652.5	81.8	18.4	654.5	2.0	72.8	26.5
ν_5 (A')	549.4	2.9	1.8	548.0	-1.4	2.8	2.1
ν_6 (A')	276.0	0.2	6.6	276.9	1.0	0.8	8.9
ν_7 (A")	1346.0	4.1	2.7	1345.1	-0.9	4.1	2.8
ν_8 (A")	1096.9	186.9	1.9	1089.6	-7.3	185.1	1.8
ν_9 (A")	277.0	0.0004	1.2	278.7	1.7	0.01	1.4
CH_3Cl							
ν_1 (A)	3109.9	24.4	147.2	3109.6	-0.3	17.3	144.7
ν_2 (A)	1369.8	13.2	0.006	1369.3	-0.4	8.2	0.7
ν_3 (A)	750.4	25.3	17.9	743.2	-7.2	23.6	15.4
ν_4 (E)	3230.5	3.6	48.9	3232.7	2.2	3.3	46.1
ν_5 (E)	1474.7	5.0	4.0	1471.7	-3.0	9.2	3.5
ν_6 (E)	1031.9	2.1	0.6	1032.7	0.7	4.1	0.8

Van der Waals vibrations: 5.0 cm^{-1}, 4.6 km mol^{-1}, 0.7 $Å^4$ amu^{-1}, 22.5 cm^{-1}, 2.1 km mol^{-1}, 0.8 $Å^4$ amu^{-1}, 26.5 cm^{-1}, 0.6 km mol^{-1}, 0.3 $Å^4$ amu^{-1}, 43.6 cm^{-1}, 0.02 km mol^{-1}, 0.05 $Å^4$ amu^{-1}, 51.2 cm^{-1}, 0.1 km mol^{-1},
0.5 $Å^4$ amu^{-1}, 69.5 cm^{-1}, 7.3 km mol^{-1}, 1.1 $Å^4$ amu^{-1}.

Table S10: Experimental vibrational frequencies for the monomer and complexes, as well as experimental complexation shifts ($\Delta\nu_{exp}$) and MP2/aug-cc-pVDZ-PP calculated complexation shifts ($\Delta\nu_{calc}$), in cm^{-1}, for the halogen bonded complex (XB) and hydrogen bonded complex (HB) of difluoroiodomethane (CHF_2I) with trimethylphosphine (TMP) dissolved in LKr at 130 K.

	Assignment	$\nu_{monomer}$	$\nu_{complex,XB}$	$\Delta\nu_{exp,XB}$	$\Delta\nu_{calc,XB}$	$\nu_{complex,HB}$	$\Delta\nu_{exp,HB}$	$\Delta\nu_{calc,HB}$
CHF_2I	ν_1	3003.3	2989.9[a]	-13.4	-12.1	2989.9[a]	-13.4	-19.6
	$\nu_5+\nu_7+\nu_8$	2993.9			-24.3			21.0
	$\nu_3+\nu_8$	2171.2	2145.2	-26.0	-23.2	2160.6	-10.6	-8.1
	$2\nu_3$	2144.1	2129.0	-15.1	-11.9	2133.9	-10.2	-7.9
	ν_7	1337.2	1335.5	-1.7	-2.3			23.5
	ν_2	1247.6	1244.0	-3.6	-1.2	1247.8	0.8	0.6
	ν_8	1107.6	1087.7	-19.9	-17.2	1101.8	-5.8	-4.2
	ν_3	1077.1	1070.7	-6.4	-6.0	1072.5	-4.6	-3.9
	ν_4	633.6	628.5	-5.1	-5.0	663.1	-0.5	-1.5
	ν_5	567.8	563.2	-4.6	-4.7	568.3	0.5	-1.6
	$2\nu_6$	536.8						
TMP	ν_{12}	2971.9	2974.6	2.7	3.0	2974.6	2.7	2.3
	ν_1	2957.7	2961.0	2.3	3.1	2961.0	2.3	2.7
	ν_{13}	2957.7	2961.0	2.3	3.5	2961.0	2.3	3.1
	ν_2	2897.2	2899.2	2.0	2.5	2899.2	2.0	2.3
	ν_{14}	2897.2	2899.2	2.0	2.5	2899.2	2.0	2.4
	ν_3	1436.6	1436.2	-0.4	-1.3	1436.2	-0.4	-0.3
	ν_{15}	1426.9	1426.1	-0.8	-1.2	1426.1	-0.8	-0.7
	ν_{16}	1418.3	1417.9	-0.4	-1.2	1417.9	-0.4	-0.3
	$\nu_{6+}\nu_{20}$	1359.4	1366.9	7.5	7.8	1366.9	7.5	6.4
	$2\nu_6$	1310.9	1314.5	3.6	2.7	1314.5	3.6	3.8
	ν_4	1295.1	1297.7	2.6	0.7	1297.7	2.6	1.0
	ν_{17}	1278.7	1280.8	2.1	0.9	1280.8	2.1	0.7
	ν_5	949.0	948.8	-0.2	-0.3	950.5	1.5	1.5
	ν_{18}	937.6	939.8	2.2	2.3	939.8	2.2	2.3
	ν_{19}	825.3	827.2	1.9	1.2	827.2	1.9	2.2
	ν_{20}	708.7	715.0	6.3	6.4	713.1	4.4	4.5
	ν_6	654.1	656.0	1.9	1.4	656.0	1.9	1.9

[a] Shoulder of TMP complex band

Table S11: Experimental vibrational frequencies for the monomer and complexes, as well as experimental complexation shifts ($\Delta\nu_{exp}$) and MP2/aug-cc-pVDZ-PP calculated complexation shifts ($\Delta\nu_{calc}$), in cm^{-1}, for the halogen bonded complex (XB) and hydrogen bonded complex (HB) of difluoroiodomethane (CHF_2I) with dimethyl sulfide (DMS) dissolved in LKr at 130 K.

	Assignment	$\nu_{monomer}$	$\nu_{complex,XB}$	$\Delta\nu_{exp,XB}$	$\Delta\nu_{calc,XB}$	$\nu_{complex,HB}$	$\Delta\nu_{exp,HB}$	$\Delta\nu_{calc,HB}$
CHF_2I	ν_1	3003.3	2994.5	-8.8	-9.3	2994.5	-8.8	9.7
	$\nu_{5+}\ \nu_{7+}\ \nu_8$	2993.9			-20.3			-4.9
	$\nu_{3+}\ \nu_8$	2170.7	2150.9	-19.8	-19.7	2163.0	-7.7	-9.9
	$2\nu_3$	2143.7	2132.7	-11.0	-10.1	2132.7	-11.0	-11.7
	ν_7	1337.3	1336.2	-1.1	-1.8	1336.2	-1.1	-1.6
	ν_2	1247.6	1247.9	0.3	-0.2	1247.9	0.3	-2.9
	ν_8	1107.3	1092.7	-14.6	-14.6	1103.6	-3.7	-4.0
	ν_3	1077.1	1072.5	-4.6	-5.0	1072.5	-4.6	-5.9
	ν_4	633.6	632.3	-1.3	-2.0	663.3	-1.3	-2.0
	ν_5	567.7	564.3	-3.4	-3.8	568.0	0.3	0.7
	$2\nu_6$	536.3	533.0	-3.3	-3.8	533.0	-3.3	-5.0
DMS	ν_1	2992.0	2994.4	2.4	1.9	2994.4	2.4	1.4
	ν_{16}	2992.0	2994.4	2.4	1.9	2994.4	2.4	2.6
	ν_{12}	2965.5	2970.3	4.8	3.7	2970.3	4.8	5.1
	ν_{17}	2920.4	2921.9	1.5	-0.2	2921.9	1.5	1.1
	ν_2	2917.3	2918.9	1.6	0.1	2918.9	1.6	1.5
		2883.8						
		2864.6	2862.4	-2.2		2862.4	-2.2	
		2856.5	2855.3	-1.2		2855.3	-1.2	
	$2\nu_9$	2838.4	2836.3	-2.1	-3.5	2836.3	-2.1	-3.7
	ν_3	1444.4	1442.8	-1.6	-2.0	1444.4	0.0	-0.8
	ν_{18}	1438.9	1437.2	-1.7	-2.6	1437.2	-1.7	-1.2
	ν_{13}	1432.8	1432.2	-0.6	-1.4	1432.2	-0.6	-1.8
	ν_4 (vw)	1331.8			-0.3			0.6
	ν_{19}	1310.4	1311.5	1.1	0.1	1311.5	1.1	-0.1
	ν_5	1030.8	1032.0	1.2	1.1	1032.0	1.2	1.5
	ν_{14}	973.3	975.3	2.0	2.3	975.3	2.0	3.0
	ν_{20}	901.8	904.0	2.2	2.2	904.0	2.2	2.5
	ν_6	696.2	694.0	-2.2	-2.8	696.2	-2.2	-2.4

Table S13: Overview of the different van 't Hoff plots constructed for the halogen bonded complex between CHF_2I and TMP or TMP-d_9 in LKr in the 120-156 K temperature interval, showing the estimated mole fractions of each monomer, range of the integrated monomer and complex bands and complex enthalpies $\Delta H°$ (LKr).

x_{CHF_2I}	x_{TMP}	Integrated CHF_2I band (cm^{-1})	Integrated TMP band (cm^{-1})	Integrated Complex band (cm^{-1})	$\Delta H°$ (LKr) [a]
1.1×10^{-4}	1.9×10^{-3}	1128-1093	3000-2930	1095-1080	-15.6(2)
6.1×10^{-5}	9.4×10^{-4}	646-622	834.4-819.5	1095-1080	-15.6(3)
1.9×10^{-4}	1.9×10^{-3} [b]	1128-1093	2263-2185	1095-1080	-15.0(1)

[a] Values are given with the standard deviation of the linear regression in parentheses.

[b] Measurement involving TMP-d_9, rather than TMP.

Table S14: Overview of the different van 't Hoff plots constructed for the hydrogen bonded complex between CHF_2I and TMP or TMP-d_9 in LKr in the 120-156 K temperature interval, showing the estimated mole fractions of each monomer, range of the integrated monomer and complex bands and complex enthalpies $\Delta H°$ (LKr).

x_{CHF_2I}	x_{TMP}	Integrated CHF_2I band (cm^{-1})	Integrated TMP band (cm^{-1})	Integrated Complex band (cm^{-1})	$\Delta H°$ (LKr) [a]
1.1×10^{-4}	1.9×10^{-3}	1128-1093	3000-2930	1110-1095	-10.40(5)
6.1×10^{-5}	9.4×10^{-4}	646-622	834.4-819.5	1109-1095	-10.3(1)
1.9×10^{-4}	1.9×10^{-3} [b]	1128-1093	2263-2185	1110-1095	-10.8(1)

[a] Values are given with the standard deviation of the linear regression in parentheses.
[b] Measurement involving TMP-d_9, rather than TMP.

Table S15: Overview of the different van 't Hoff plots constructed for the halogen bonded complex between CHF_2I and DMS or DMS-d_6 in LKr in the 120-156 K temperature interval, showing the estimated mole fractions of each monomer, range of the integrated monomer and complex bands and complex enthalpies $\Delta H°$ (LKr).

x_{CHF_2I}	x_{DMS}	Integrated CHF_2I band (cm^{-1})	Integrated DMS band (cm^{-1})	Integrated Complex band (cm^{-1})	$\Delta H°$ (LKr) [a]
3.8×10^{-5}	1.9×10^{-3}	1263-1234	997-955	CHF_2I ν_8 (1092.6)	-12.0(2)
1.1×10^{-4}	1.9×10^{-3} [b]	1263-1232	2275-2195	CHF_2I ν_8 (1092.6) [c]	-11.3(3)
1.9×10^{-4}	1.9×10^{-3}	1262-1238	1322-1302	CHF_2I ν_8 (1092.6) [c]	-10.8(2)
1.9×10^{-4}	1.9×10^{-3} [b]	1262.5-1235	2280-2185	CHF_2I ν_8 (1092.6) [c]	-11.1(1)

[a] Values are given with the standard deviation of the linear regression in parentheses.
[b] Measurement involving DMS-d_6, rather than DMS.
[c] Intensity obtained from a band fit analysis.

Table S16: Overview of the different van 't Hoff plots constructed for the hydrogen bonded complex between CHF_2I and DMS or DMS-d_6 in LKr in the 120-156 K temperature interval, showing the estimated mole fractions of each monomer, range of the integrated monomer and complex bands and complex enthalpies $\Delta H°$ (LKr).

x_{CHF_2I}	x_{DMS}	Integrated CHF_2I band (cm^{-1})	Integrated DMS band (cm^{-1})	Integrated Complex band (cm^{-1})	$\Delta H°$ (LKr) [a]
3.8×10^{-5}	1.9×10^{-3}	1263-1234	997-955	1114-1090	-8.0(2)
1.1×10^{-4}	1.9×10^{-3} [b]	1124-1093	2275-2195	1118-1090	-7.1(3)
1.9×10^{-4}	1.9×10^{-3}	1262.1238	1322-1302	1116-1091	-7.4(1)
1.9×10^{-4}	1.9×10^{-3} [b]	1262.5-1235	2280-2185	1114-1089	-8.3(2)

[a] Values are given with the standard deviation of the linear regression in parentheses.
[b] Measurement involving DMS-d_6, rather than DMS.

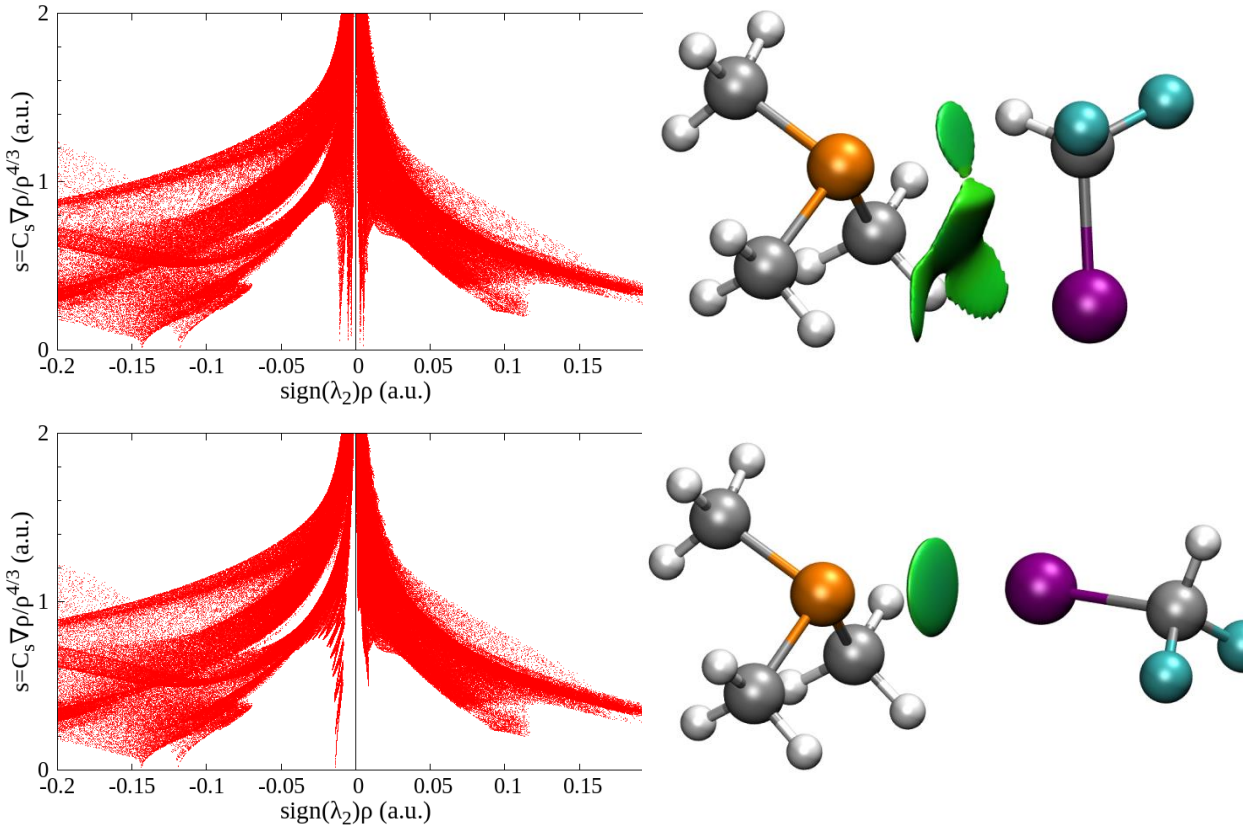

Figure S1: Plots of the reduced density gradient versus the electron density multiplied by the sign of the second Hessian eigenvalue (left) and gradient isosurfaces (s = 0.5 a.u., right) for the hydrogen bonded complex (top) and the halogen bonded complex (bottom) between CHF_2I and trimethylphosphine.

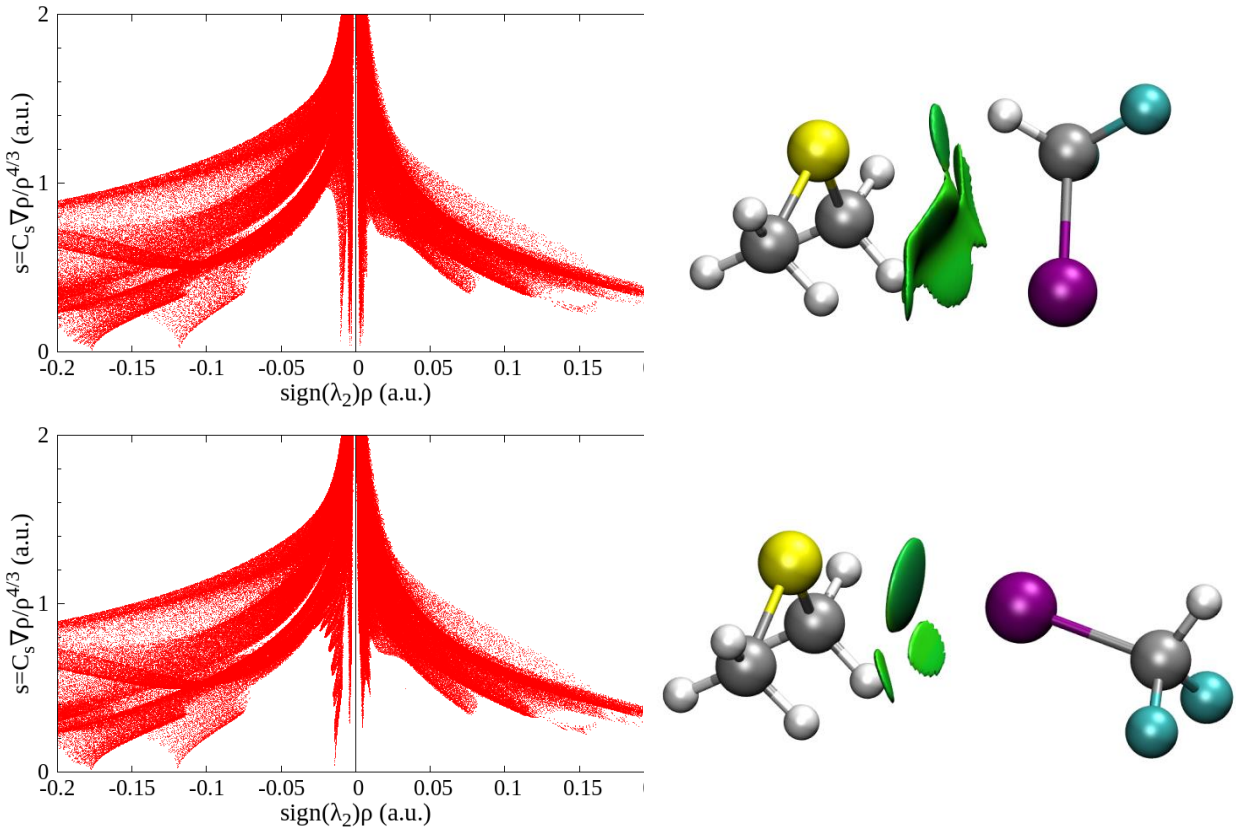

Figure S2: Plots of the reduced density gradient versus the electron density multiplied by the sign of the second Hessian eigenvalue (left) and gradient isosurfaces (s = 0.5 a.u., right) for the hydrogen bonded complex (top) and the halogen bonded complex (bottom) between CHF_2I and dimethyl sulfide.

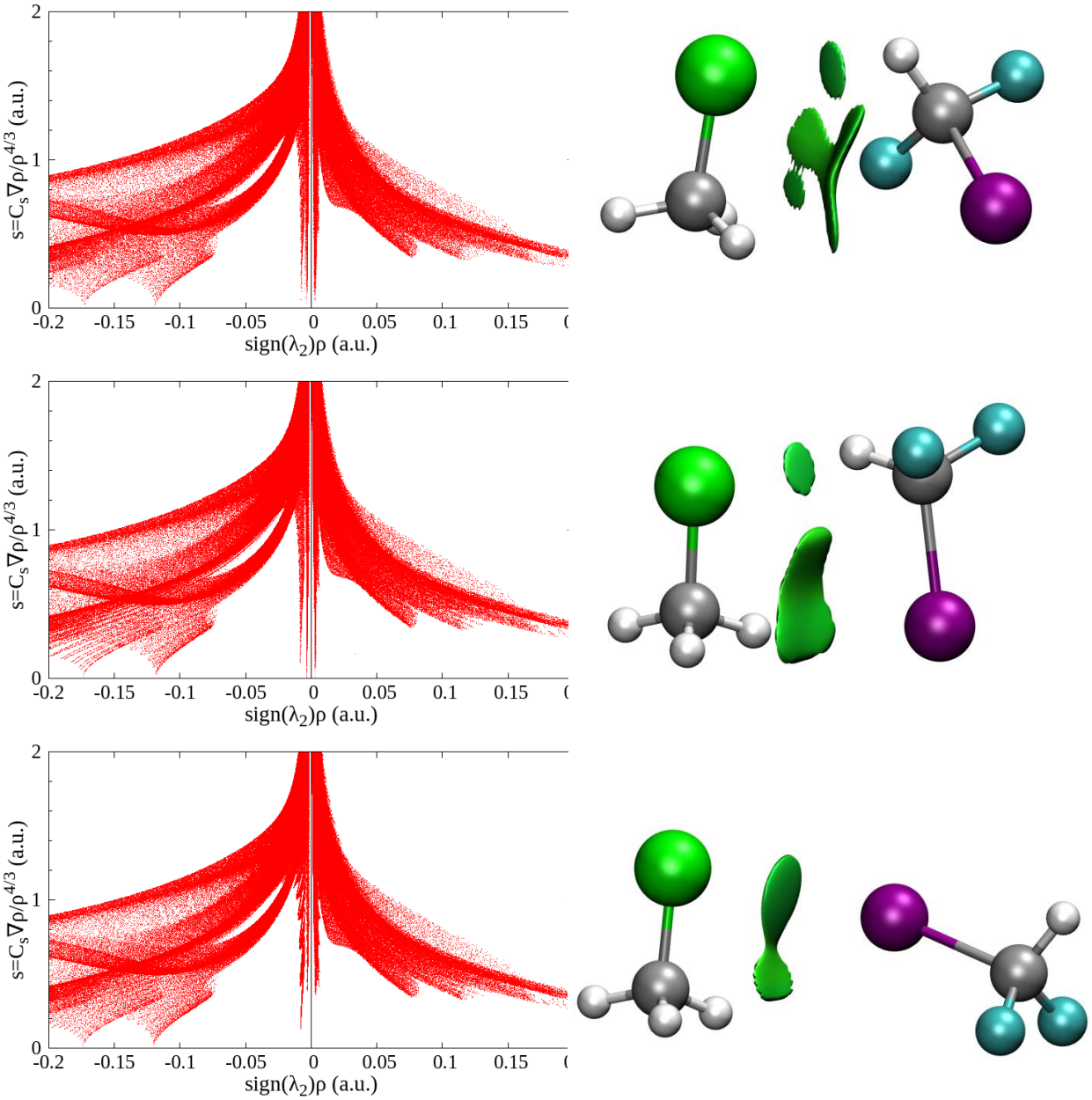

Figure S3: Plots of the reduced density gradient versus the electron density multiplied by the sign of the second Hessian eigenvalue (left) and gradient isosurfaces (s = 0.5 a.u., right) for the hydrogen bonded complexes with a secondary C-H···F (top) or C-H···I interaction (middle) and the halogen bonded complex (bottom) between CHF_2I and CH_3Cl.

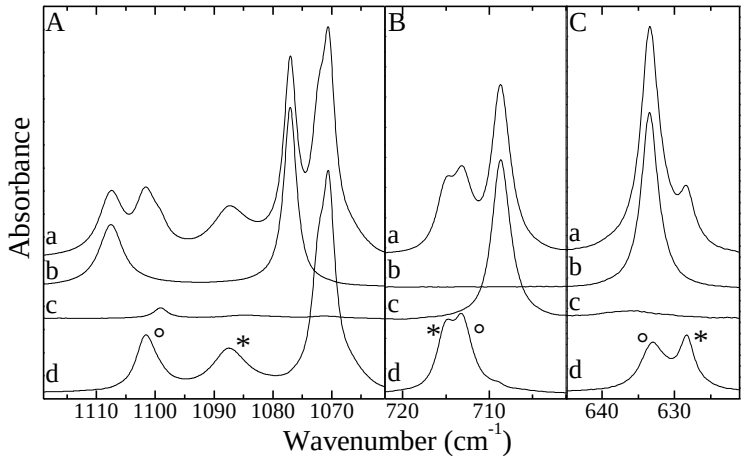

Figure S4: Infrared spectra of selected spectral regions for the mixtures of difluoroiodomethane with trimethylphosphine dissolved in LKr at 130 K. In each panel, trace *a* represents the mixed solution, while traces *b* and *c* show the rescaled spectra of the solutions containing only difluoroiodomethane or trimethylphosphine, respectively. Trace *d* represents the spectrum of the complex which is obtained by subtracting the rescaled traces *b* and *c* from trace *a*. Bands due to the halogen and hydrogen bonded complexes observed in traces *d* are marked with an asterisk (*) or open circle (°), respectively. Estimated mole fractions of the solutions of the mixtures are 5.6×10^{-5} for CHF_2I and 3.8×10^{-3} for TMP in panel A, 9.4×10^{-4} for CHF_2I and 9.4×10^{-4} for TMP in panel B and 5.6×10^{-5} for CHF_2I and 2.4×10^{-3} for TMP-d_9 in panel C.

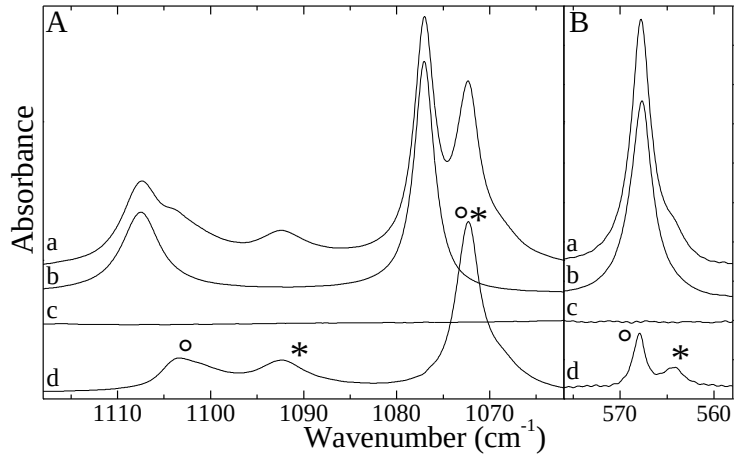

Figure S5: Infrared spectra of selected spectral regions for the mixtures of difluoroiodomethane with dimethyl sulfide dissolved in LKr at 130 K. In each panel, trace *a* represents the mixed solution, while traces *b* and *c* show the rescaled spectra of the solutions containing only difluoroiodomethane or dimethyl sulfide, respectively. Trace *d* represents the spectrum of the complex which is obtained by subtracting the rescaled traces *b* and *c* from trace *a*. Bands due to the halogen and hydrogen bonded complexes observed in traces *d* are marked with an asterisk (*) or open circle (°), respectively. Estimated mole fractions of the solutions of the mixtures are 5.6×10^{-5} for CHF_2I and 3.8×10^{-3} for DMS in panel A and 9.4×10^{-4} for CHF_2I and 1.9×10^{-3} for DMS in panel B.

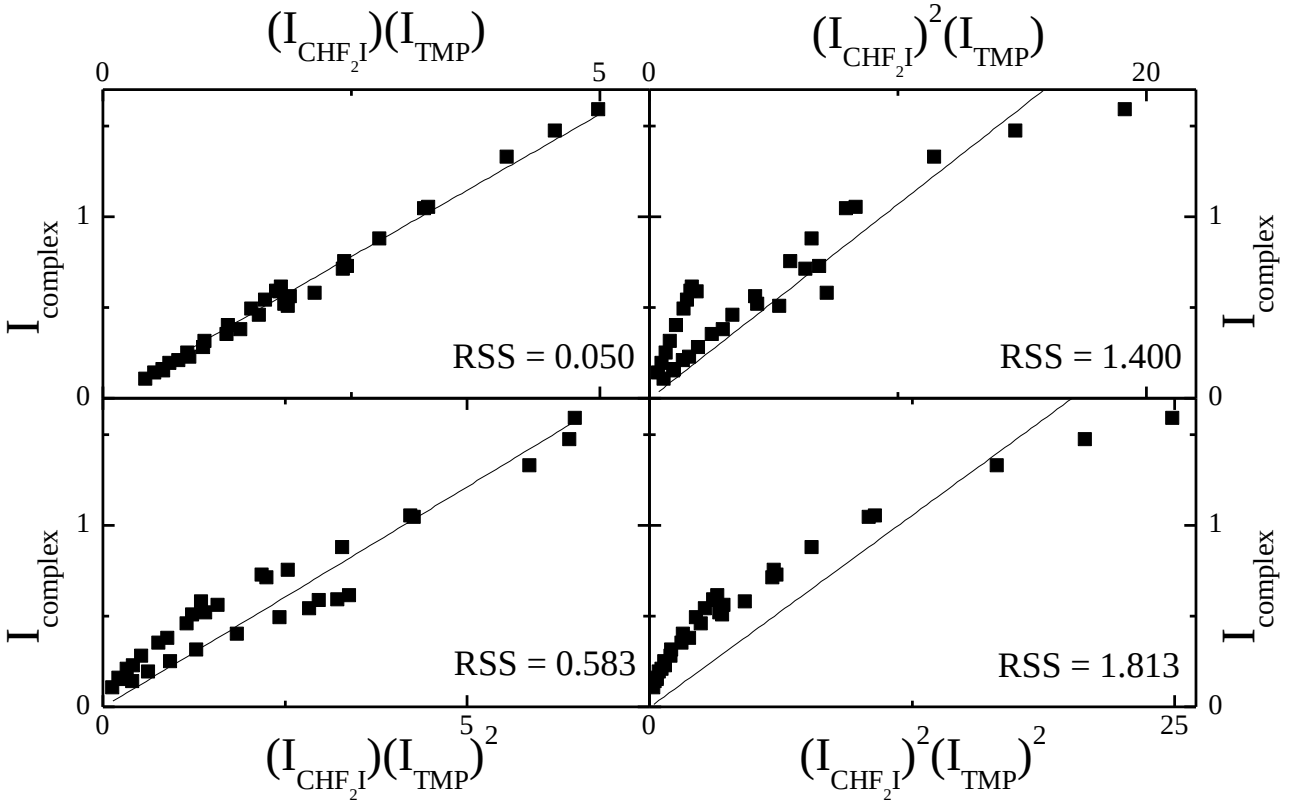

Figure S6: Concentration study plots of the CHF_2I·TMP halogen bonded complex at 130 K in LKr. Integrated intensity of the complex is plotted against the product of monomer intensities $(I_{CHF_2I})^m(TMP)^n$. Top left: $m = 1, n = 1$, top right: $m = 2, n = 1$, bottom left $m = 1, n = 2$ and bottom right $m = 2, n = 2$. Additionally, residual sum of square values (RSS) have been included.

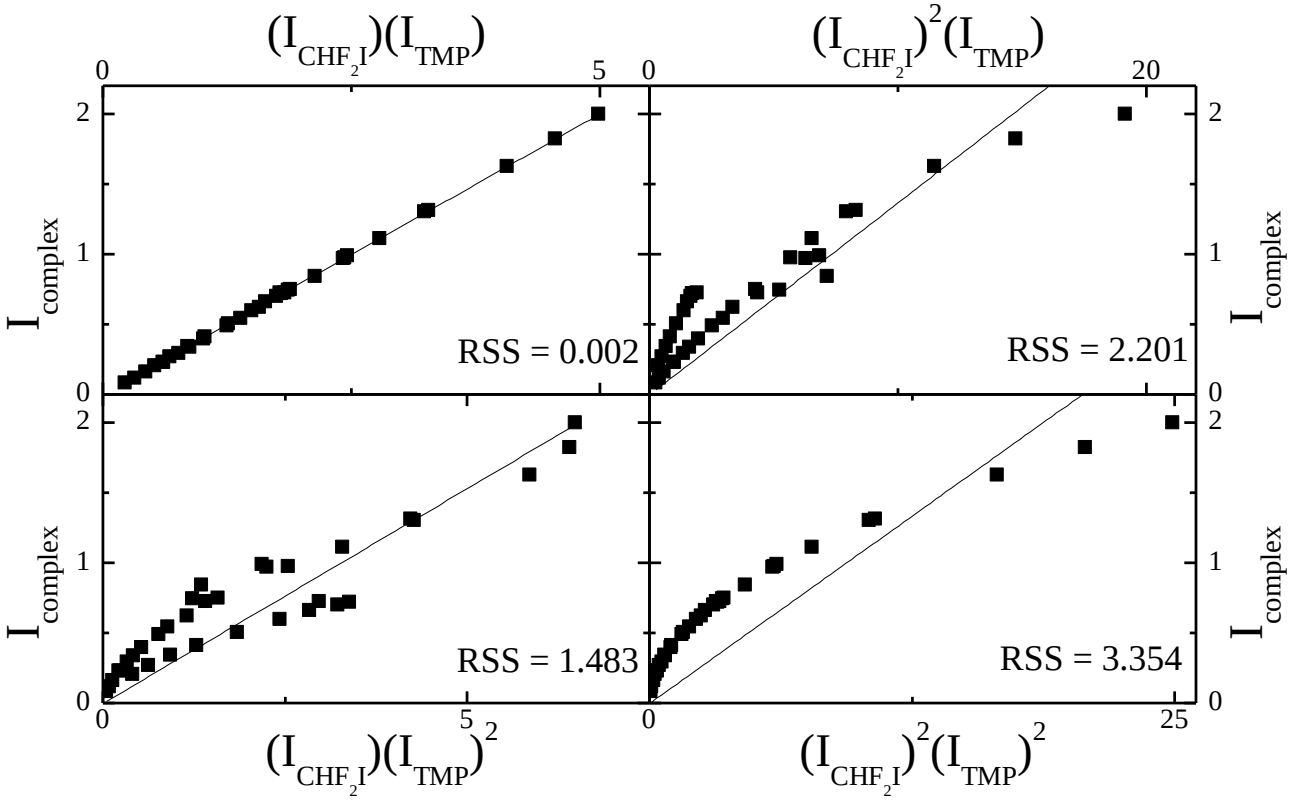

Figure S7: Concentration study plots of the CHF_2I·TMP hydrogen bonded complex at 130 K in LKr. Integrated intensity of the complex is plotted against the product of monomer intensities $(I_{CHF_2I})^m(TMP)^n$. Top left: $m = 1, n = 1$, top right: $m = 2, n = 1$, bottom left $m = 1, n = 2$ and bottom right $m = 2, n = 2$. Additionally, residual sum of square values (RSS) have been included.

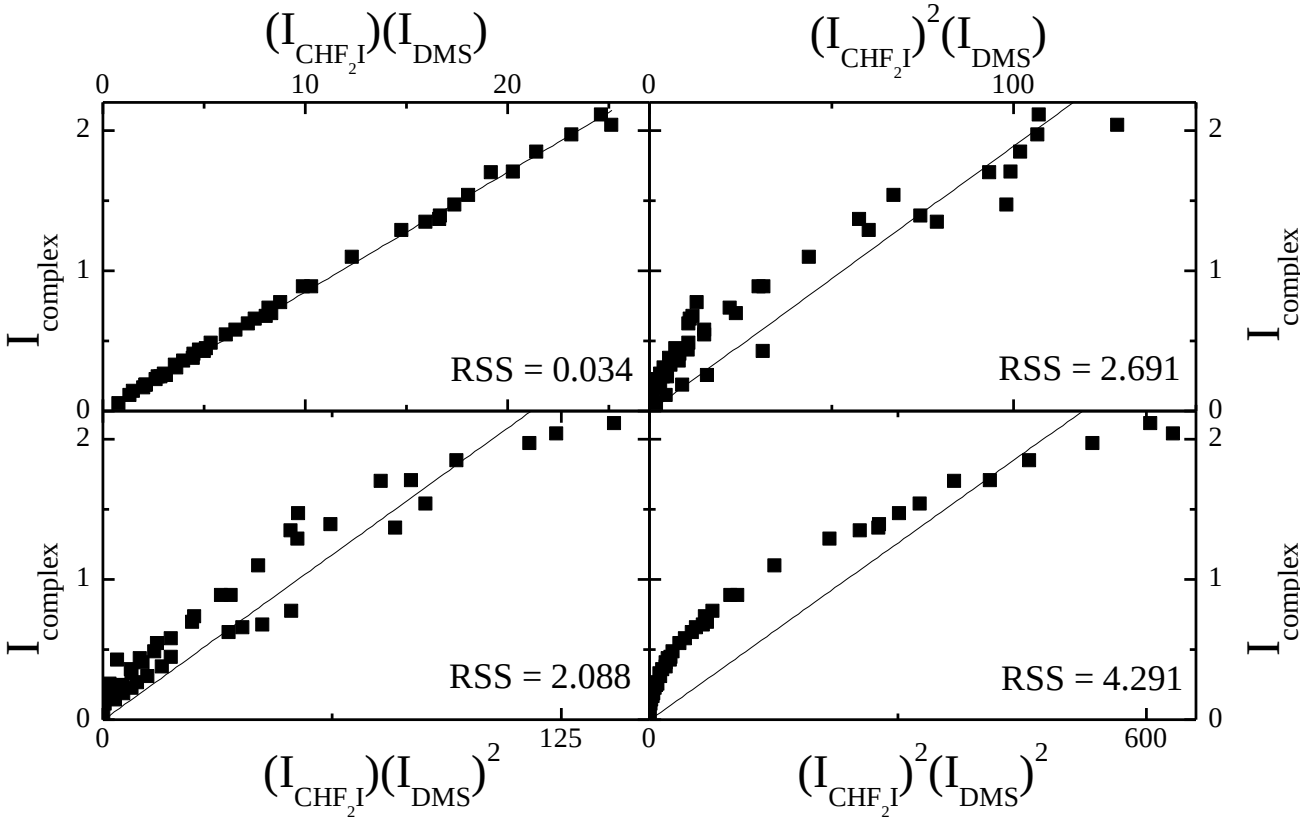

Figure S8: Concentration study plots of the CHF_2I·DMS halogen bonded complex at 130 K in LKr. Integrated intensity of the complex is plotted against the product of monomer intensities $(I_{CHF_2I})^m(DMS)^n$. Top left: $m = 1, n = 1$, top right: $m = 2, n = 1$, bottom left $m = 1, n = 2$ and bottom right $m = 2, n = 2$. Additionally, residual sum of square values (RSS) have been included.

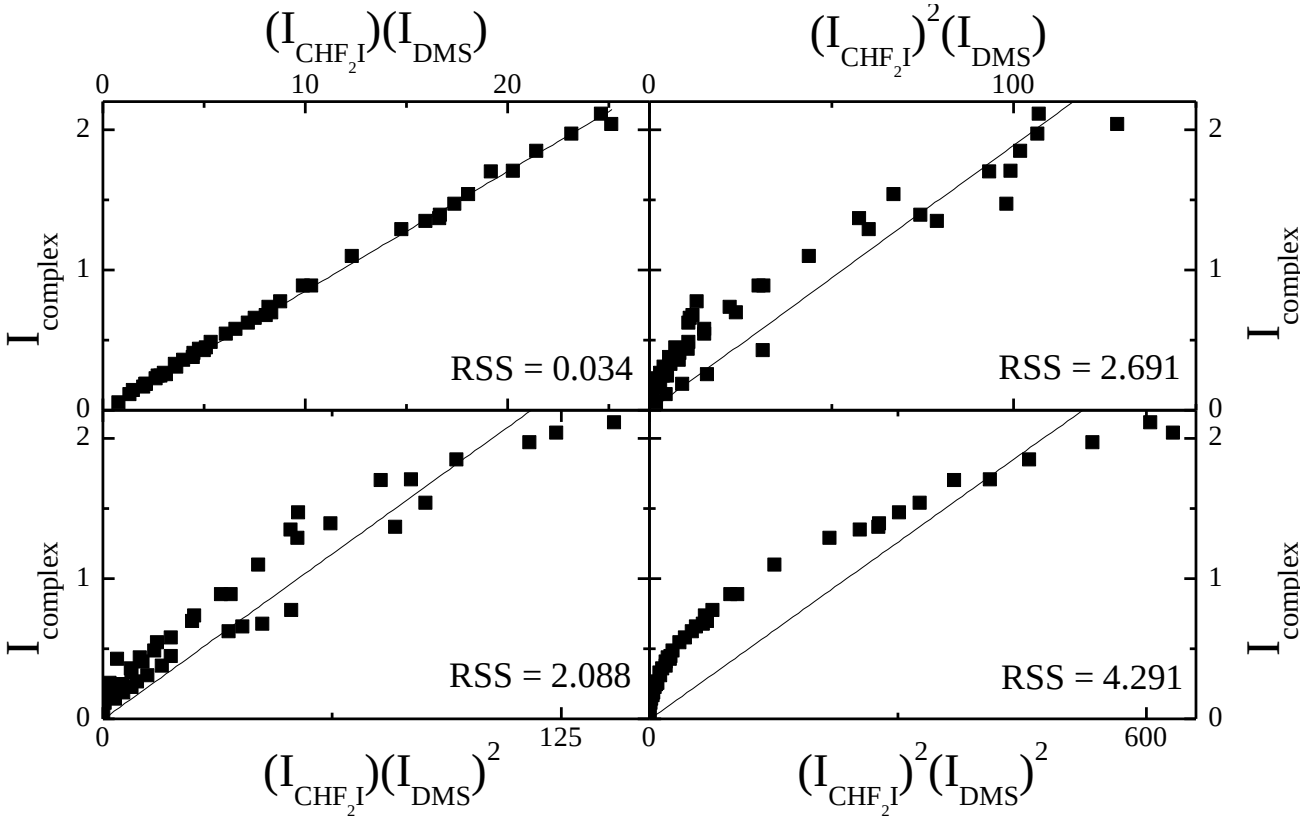

Figure S9: Concentration study plots of the CHF_2I·DMS hydrogen bonded complex at 130 K in LKr. Integrated intensity of the complex is plotted against the product of monomer intensities $(I_{CHF_2I})^m(DMS)^n$. Top left: $m = 1, n = 1$, top right: $m = 2, n = 1$, bottom left $m = 1, n = 2$ and bottom right $m = 2, n = 2$. Additionally, residual sum of square values (RSS) have been included.

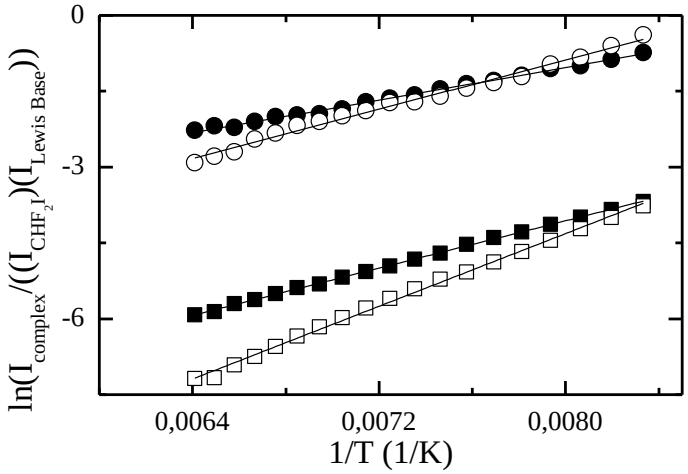

Figure S10: Typical van 't Hoff plots of the hydrogen bonded complexes (filled) and halogen bonded complexes (hollow) of CHF_2I with dimethyl sulfide (round) and trimethylphosphine (square) in LKr.

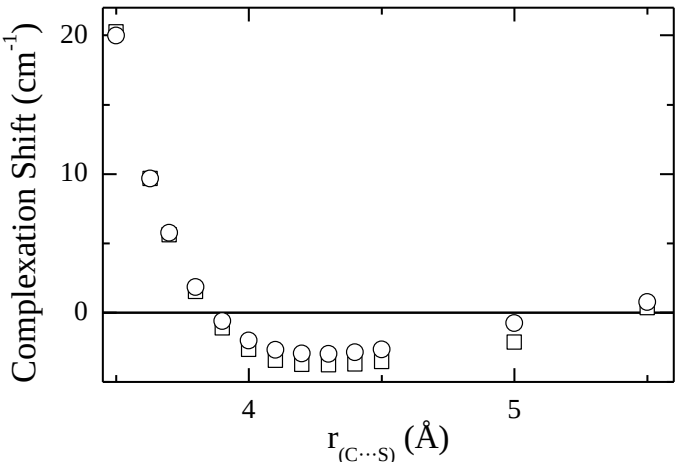

Figure S11: Complexation shifts (in cm^{-1}) of the CHF_2I ν_1 mode plotted against the C···S distance (in Å) for the partially optimized hydrogen bonded complex with the C-H···S angle (□) and C-H···S angle and C-H···S-C dihedral angle (○) from the equilibrium geometry.

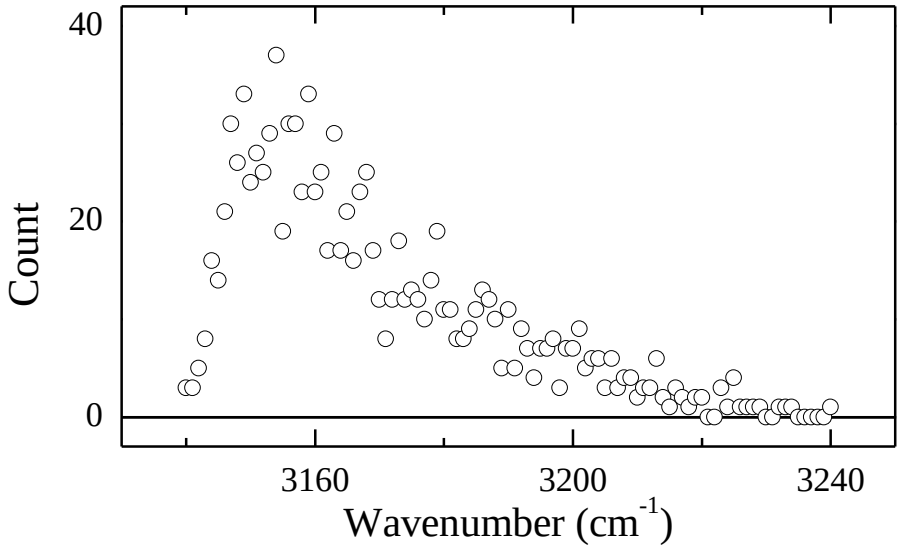

Figure S12: Distribution of MP2/aug-cc-pVDZ-PP *ab initio* frequencies for the CH stretching mode of the hydrogen bonded complex between CHF_2I and DMS-d_6 at 130 K, obtained from a Monte Carlo sample of the internal coordinates describing the relative orientation of both molecules. Division of the frequencies was made using a bin-width of 1 wavenumber.

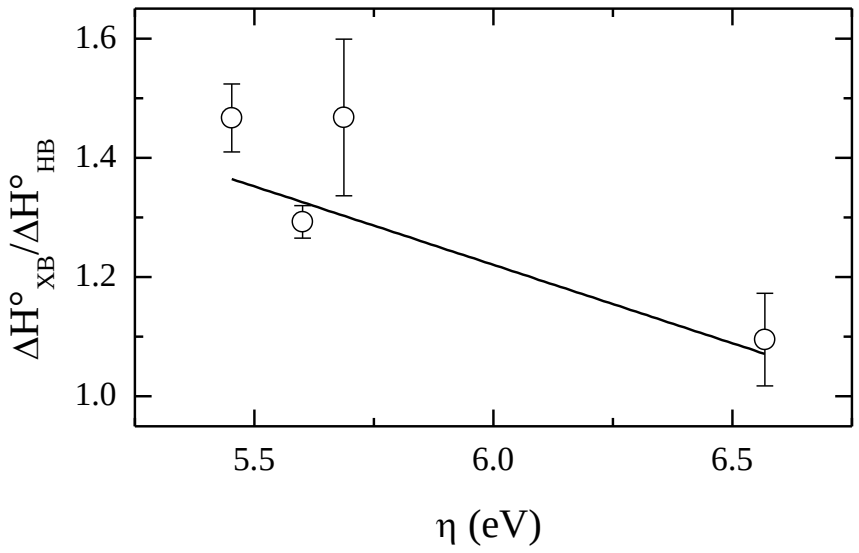

Figure S13: Plot of the enthalpy ratio of $\frac{\Delta H°_{XB}}{\Delta H°_{HB}}$ versus chemical hardness η (in eV), as calculated using the method of Tozer et al. for the complexes formed between difluoroiodomethane and the Lewis bases trimethylamine, dimethyl ether, trimethylphosphine and dimethyl sulfide.